

# 1 Systematic mining and genetic characterization of regulatory factors 2 for wheat spike development

3 Xuelei Lin<sup>1,8</sup>, Yongxin Xu<sup>1,2,8</sup>, Dongzhi Wang<sup>1,8</sup>, Yiman Yang<sup>1,3</sup>, Xiaoyu Zhang<sup>1,2</sup>,  
4 Xiaomin Bie<sup>4</sup>, Hongzhe Wang<sup>1</sup>, Jiafu Jiang<sup>3</sup>, Yiliang Ding<sup>5</sup>, Fei Lu<sup>1,2,7</sup>, Xueyong  
5 Zhang<sup>6</sup>, Xiansheng Zhang<sup>4</sup>, Xiangdong Fu<sup>1,2</sup>, Jun Xiao<sup>1,2,7\*</sup>

6

7 <sup>1</sup> Key Laboratory of Plant Cell and Chromosome Engineering, Institute of Genetics and  
8 Developmental Biology, Chinese Academy of Sciences, Beijing 100101, China

9 <sup>2</sup> University of Chinese Academy of Sciences, Beijing 100049, China

10 <sup>3</sup> Nanjing Agricultural University, Nanjing, Jiangsu, 210095, China

11 <sup>4</sup> Shandong Agricultural University, Tai'an, Shandong, 271018, China

12 <sup>5</sup> Department of Cell and Developmental Biology, John Innes Centre, Norwich Research  
13 Park, Norwich NR4 7UH, UK

14 <sup>6</sup> Institute of Crop Sciences, Chinese Academy of Agricultural Sciences, 100081, China

15 <sup>7</sup> Centre of Excellence for Plant and Microbial Science (CEPAMS), JIC-CAS, 100101,  
16 China

17 <sup>8</sup> These authors contributed equally to this article.

18 \*Correspondence: Jun Xiao ([jxiao@genetics.ac.cn](mailto:jxiao@genetics.ac.cn))

19

## 20 **Abstract**

21 Spike architecture largely affects grain number embraced, which is a key factor  
22 influencing wheat grain yield. Here, we systematically explore the genetic regulation  
23 network governing wheat spike development by integration of multi-omic data with  
24 population genetics. Transcriptome and epigenome profile of shoot apex at eight  
25 developmental stages were generated. Gain-of-chromatin accessibility and changes of  
26 H3K27me3 coordinately associate with the progressive transcriptome alteration for  
27 flowering. A core transcriptional regulation network (TRN) that likely drives various  
28 meristematic cell identities transition to form spike was constructed. Integration of the

29 TRN and genome-wide association analysis (GWAS), 260 transcription factors (TFs)  
30 were identified, including 52 characterized factors in crops, but mostly unstudied.  
31 Multi-layer regulatory module among *TaSPL6*, *TaMADS34* and *TaMADS14* suggested  
32 by TRN was further validated experimentally. About 85 novel TFs contain high impact  
33 mutant lines in KN9204 TILLING library. Of them, 44 TFs with homozygous mutation,  
34 including NAC, bHLH, MYB, and WRKY, show altered spike architecture. In  
35 particular, *TaMYB4-A* positively regulates fertile spikelet number likely via regulating  
36 hormones homeostasis or signaling, while acting downstream of- and repressed by  
37 WFZP. The elite allele of *TaMYB4-A*, with higher expression and more fertile spikelet,  
38 was selected during breeding process in China. Collectively, we present invaluable  
39 resource of high-confidence regulators and novel strategy for understanding the genetic  
40 regulation of wheat spike development systematically.

41

42 **Key words:** Spike architecture, multi-omics, GWAS, TRN, MYB

43

## 44 **Introduction**

45 Wheat (*Triticum aestivum*) is a major crop worldwide and provides about 20% of the  
46 daily calories and proteins consumed by human population. Yield is a polygenic  
47 complex quantitative trait composed of multiple elements including fertile tiller per  
48 area, grain number per spike (GNPS) and grain weight (Xiao et al., 2022). GNPS is  
49 determinate by the architecture of spike/inflorescence, which involves the number and  
50 arrangement of spikelet and fertile florets within spikelet. The spike architecture is  
51 shaped by endogenous developmental programs as well as environmental conditions  
52 (Gao et al., 2019; Lee et al., 2019; Qi et al., 2019).

53

54 During seedling stage, shoot apex meristem (SAM) constitutively produce primordium  
55 of leaves, nodes and internodes. The bract leaf primordia first appeared on the growth  
56 cone to form a single edge (SR) structure, and then the spikelet meristem (SM) was  
57 formed in the upper part of the bract to enter into double ridge (DR) stage, which is also

58 a symbol for flowering transition. SM gradually differentiates and enlarges from the  
59 middle of inflorescence to both ends. After formation of apical SM, the maximum  
60 number of spikelets is reached. Following the completion of spikelet differentiation, the  
61 lemma primordium (floral primordia differentiation stage) is formed, then it  
62 differentiates to produce pistil primordium and pollen sacs (floral organ primordia  
63 differentiation stage), and finally enters the booting stage (Bonnett, 1936). Throughout  
64 wheat spike development, SM differentiation during and after DR stage determines the  
65 spikelet number per spike (SNS) (Dobrovolskaya et al., 2015; Li et al., 2019; Li et al.,  
66 2021).

67

68 Much progresses have been made in the molecular regulation of cereal inflorescence  
69 architecture, including rice, maize and wheat (Gao et al., 2019; Yuan et al., 2020). In  
70 general, several steps are critical for the inflorescence structure, such as the duration of  
71 inflorescence development, the initiation, arrangement and terminal of spikelets, as  
72 well as the fertility of spikelet and floret (Yuan et al., 2020). In wheat, flowering time  
73 regulator such as *Photoperiod-1* (*Ppd-1*), *FLOWERING LOCUS T1* (*FT1*), *FT2*  
74 coordinately regulate the transition of SAM to inflorescence meristem (IM) and the  
75 duration of spike development, which in turn affects the paired spikelet formation  
76 (Boden et al., 2015; Finnegan et al., 2018). *TEOSINTE BRANCHED1* (*TB1*) encoding  
77 a TCP transcription factor, controls lateral branching in maize (Doebley et al., 1997).  
78 In wheat, TaTB1 interacts with FT1 to control the production of paired spikelets via  
79 regulating *VRN1* expression (Dixon et al., 2018). *VERNALIZATION1* (*VRN1*) and the  
80 other orthologs of AP1/FUL-like factor, *FRUITFULL2* (*FUL2*), and *FUL3* are required  
81 synergistically for initiation and maintenance of the SM identity (Li et al., 2019).  
82 Overexpression of *PANICLE PHYTOMER2* (*TaPAP2*), a MADS box TF coding gene  
83 in wheat, inhibits SM formation and reduces SNS (Wang et al., 2017). While *WHEAT*  
84 *ORTHOLOG OF APO1* (*WAPO1*) affects SNS by regulating the timing of terminal  
85 spikelet formation (Kuzay et al., 2022; Kuzay et al., 2019). *Q* (*AP2L5*), which encodes  
86 an APETALA 2 (AP2) TF, can significantly reduce the SNS when loss-of-function,  
87 possibly due to the premature transition of the spike meristem to terminal spikelets

88 (Debernardi et al., 2020). Overexpression of *TERMINAL FLOWER 1 (TaTFL1)-2D*  
89 delayed the terminal spikelet formation and increased SNS, while *Grain Number*  
90 *Increase 1 (GNI1)* played the opposite role on determining SNS (Sakuma et al., 2019;  
91 Wang et al., 2017). (Wang et al., 2017; Sakuma et al., 2019). *WFZP*, a homologous of  
92 rice *FRIZZY PANICLE (FZP)*, determines the SNS and the floret meristem fate partially  
93 by *VRN1* and *HOMEobox4 (TaHOX4)* (Li et al., 2021), as well as by inhibiting the  
94 repressor of spikelet formation gene *TaBA1* through epigenetic modification factors  
95 *TaHDA1* and *TaLHP1* (Du et al., 2021). Several *SQUAMOSA* promoter-binding  
96 protein-like (SPL) and MADS-box TFs are involved in the floral organ formation and  
97 regulate floret fertility, such as *TaSPL13-B* (Li et al., 2020), *TaSPL14* (Cao et al., 2021),  
98 *TaAGL6-A* (Kong et al., 2022). Besides of the key TFs that mediating the meristem  
99 identity switch, factors in auxin and cytokinin (CK) hemostasis also play important role  
100 in regulation of spike development in wheat, such as *TaCYP78A5* and *TaCKX2.1*,  
101 *TaCKX2.2* (Guo et al., 2022; Jablonski et al., 2020; Jablonski et al., 2021; Qi et al.,  
102 2019).

103  
104 The factors identified above are mainly through homologous cloning or forward genetic  
105 mapping from mutants or bi-parental population. Recently, population genetics has  
106 flourished owing to the sequencing technology innovation (Sehgal and Dreisigacker,  
107 2022). Large-scale GWAS analysis was performed among landmark cultivars with  
108 single nucleotide polymorphism (SNP) generated with genotyping-by-sequencing  
109 (GBS) (Pang et al., 2020), whole genome resequencing (Hao et al., 2020), or exome  
110 capture sequencing (Li et al., 2022a). Various genetic loci were associated with spike  
111 developmental related traits, such as spike length (SL), SNS, GNPS, grain setting and  
112 spike compactness (Pang et al., 2020; Sun et al., 2017). However, wheat is an  
113 allohexaploid of large genome plant with generally triple genes number, large  
114 proportion of intergenic regions, more complex sub-genome interaction, and long LD  
115 intervals (Hao et al., 2020; Li et al., 2022a; Pang et al., 2020), which greatly reduced  
116 the accuracy of association study (Huang and Han, 2014). Other types of information,  
117 such as genes expression network provides different filter for identification of key

118 regulators, as proved by previous studies (Li et al., 2018; VanGessel et al., 2022; Wang  
119 et al., 2017).

120

121 Here, we carried out a time serial profiling of transcriptome and epigenome at shoot  
122 apex in elite wheat cultivar Kenong 9204 (KN9204), to understand how chromatin  
123 landscape is coordinated with transcriptome dynamics during the process of spike  
124 formation. More importantly, we integrate genes co-expression and regulatory network  
125 with GWAS/QTL to identify key factors shaping wheat spike architecture, and further  
126 validate and do in-depth analysis to uncover the potential regulators' function.

127

## 128 **Results**

### 129 **A transcriptome and chromatin landscape atlas for wheat spike formation**

130 To understand the transcriptional regulation for wheat spike development, shoot tips of  
131 eight distinct stages of cultivar KN9204 were sampled, including SAM, elongation  
132 stage (EL), SR, DR, spikelet meristem initiation stage (SMI), glume primordium  
133 differentiation stage (GPD), floral meristem initiation stage (FMI), floral organ  
134 primordia differentiation stage (FOP) (Figure 1A). RNA-seq and the Assay for  
135 Transposase Accessible Chromatin with high-throughput sequencing (ATAC-seq)  
136 were used to profile global gene expression, chromatin accessibility with two or three  
137 bio-replicates (Figure 1A and Supplemental Figure 1A) (Buenrostro et al., 2015; Kaya-  
138 Okur et al., 2019; Zhao et al., 2022).

139

140 In total, 58,875 high-confidence genes were found to express at least in one stage  
141 ( $TPM > 0.5$ ) (Supplemental Table 1). The principal component analysis (PCA) showed  
142 that the eight stages could be subdivided into two major categories, as vegetative group  
143 including SAM, EL, SR, DR and reproductive group including SMI, GPD, FMI and  
144 FOP (Figure 1B). More differential expressed genes (DEGs) between adjacent stages  
145 occurs at morphological transition points, such as DR to SMI, SMI to GPD, FMI to  
146 FOP, when spikelet meristem, glume primordial and floral organ primordial initiate

147 respectively (Figure 1C and Supplemental Table 2). Stage-specific expressed genes are  
148 identified via clustering (Figure 1D). Known factors involved in flowering time  
149 regulation and inflorescence development is highlighted from specific cluster. For  
150 instance, flowering time gene *TaPPD1* in cluster2 is expressed before floral transition  
151 from SAM to DR (Boden et al., 2015; Perez-Gianmarco et al., 2020); *WAPO1*, required  
152 for the maintenance of SM activity, is highly expressed at SMI (Kuzay et al., 2022);  
153 *TaTFL1* and *WFZP*, involved in terminal spikelet formation and floret fate, are  
154 expressed at GPD and FMI (Li et al., 2021; Wang et al., 2017); floral organ regulator  
155 *TaAGL6* is highly expressed at FOP (Kong et al., 2022) (Figure 1D). Besides, various  
156 members of SPL family TF (*TaSPL9/12*, *TaSPL1*, *TaSPL14*, and *TaSPL8/16*) are  
157 highly expressed at different stages (Figure 1D), consistent with recent report (Li et al.,  
158 2022b). Such transcriptome pattern correlates with the morphological characteristic of  
159 individual stage, indicating our sampling could capture the dynamic gene expression  
160 profile during wheat spike development.

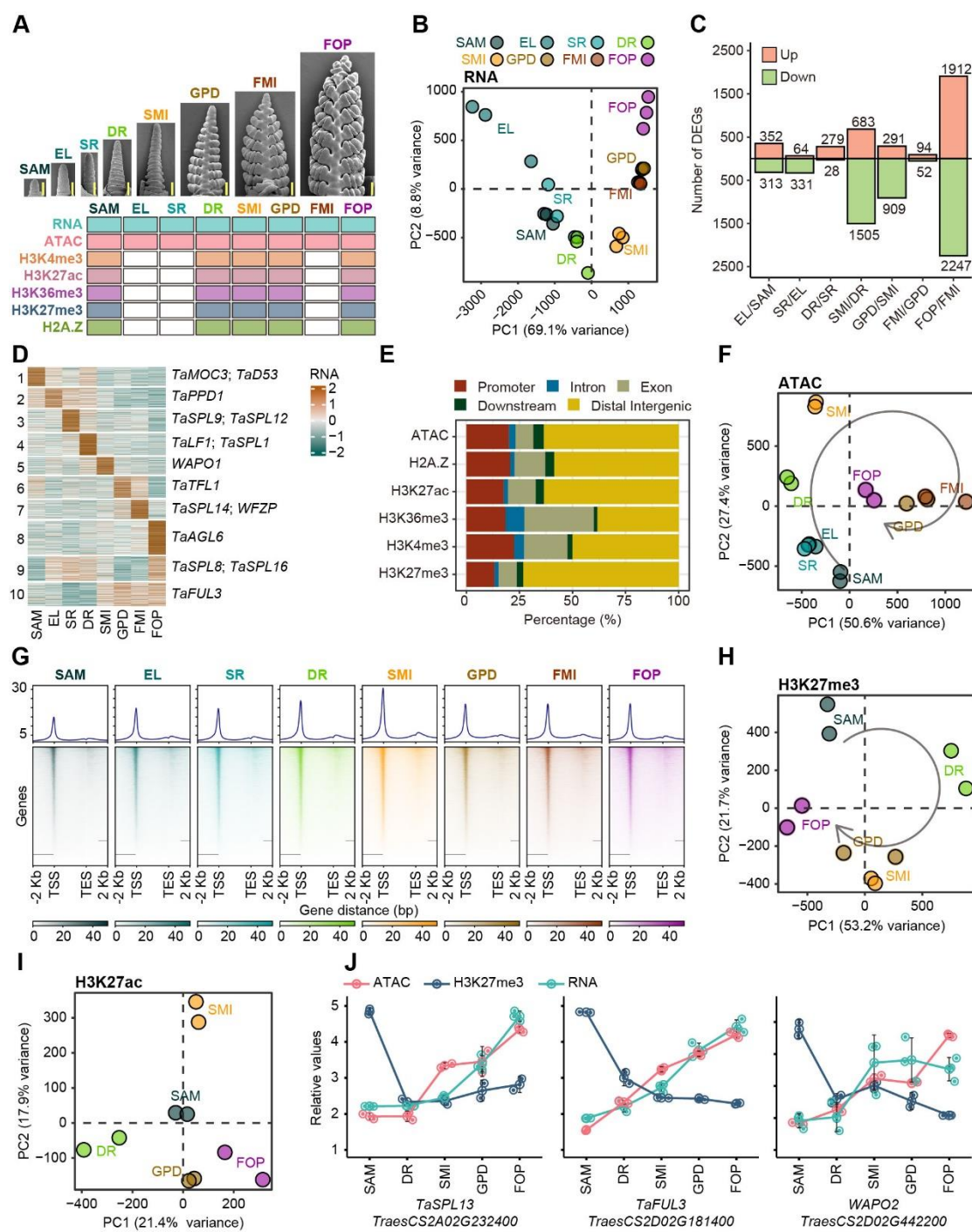
161  
162 As our previous report (Zhao et al., 2022), accessible chromatin is mainly located in  
163 the distal intergenic regions and promoters (Figure 1E). ATAC-seq peak intensity at  
164 genic region, in particular around TSS, is positively correlated with gene expression  
165 (Supplemental Figure 1B). Unsupervised PCA revealed a continuous trajectory of  
166 chromatin accessibility dynamics during wheat spike development (Figure 1F). Eight-  
167 stages could partition into five sub-clusters, as vegetative cluster before flowering  
168 including SAM, EL, SR, flowering transition stage (DR), inflorescence initiation  
169 (SMI), spikelet meristem formation (FMI, GPD) and floret meristem formation (FOP)  
170 (Supplemental Figure 1C). A globally increasing of chromatin accessibility at genic  
171 regions was observed from vegetative cluster to flowering transition and inflorescence  
172 initiation, whereas, declined during spikelet and floret formation (Figure 1G and  
173 Supplemental Figure 1D).

174  
175 Based on the chromatin accessibility dynamics, SAM, DR, SMI, GPD and FOP stages  
176 were chosen for histone modification profiling via Cleavage Under Targets and

177 Tagmentation (CUT&Tag) (Figure 1A) (Zhao et al., 2022). In general, H3K27ac,  
178 H3K4me3 and H3K36me3 intensity around TSS are positively correlated with gene  
179 expression, while H3K27me3 is enriched at gene body of no/low expressed genes  
180 (Figure 1E and Supplemental Figure 1B). H3K27me3 and H3K36me3 was mutually  
181 exclusive for each other, H3K4me3 and H3K27ac was positively correlated, whereas,  
182 histone variants H2A.Z was overlapped with both active H3K27ac and H3K4me3 and  
183 repressive H3K27me3, but depleted with H3K36me3 (Supplemental Figure 1E and  
184 Supplemental Table 3). The PCA and cluster analyses showed that various histone  
185 modifications had stage-specific transitions during different developmental stages  
186 (Figures 1H and 1I and Supplemental Figures 1F-1H). Of note, H3K27me3 presents  
187 continuous trajectory while others are not, suggesting higher correlation with  
188 transcriptional profile dynamics (Figure 1H). Indeed, H3K27me3 abundance and  
189 chromatin accessibility jointly affect different genes expression pattern during spike  
190 development (Figure 1J).

191  
192 Taken together, we have generated transcriptomic and epigenomic profile of shoot apex  
193 at important stages during wheat spike formation, which can facilitate elucidating the  
194 transcriptional regulatory insights for shaping wheat inflorescence architecture.

195



196

197 **Figure 1. Charting transcriptome and chromatin landscapes during wheat spike  
198 development.**

199 (A) Scanning electronic micrographs (SEM) of young spikes in eight developmental  
200 stages and experimental design. SAM, shoot apical meristem; EL, elongation stage;  
201 SR, single ridge; DR, double ridge; SMI, spikelet meristem initiation; GPD, glume  
202 primordium differentiation; FMI, floral meristem initiation; FOP, floral organ  
203 primordium differentiation. Bar= 200  $\mu$ m.

204 (B) Principal component analysis (PCA) of transcriptome showing distinct  
205 development stages. Each dot represents one sample. Color represents the different

206 stages during spike development. Three bio-replicates were sequenced for each  
207 stage.  
208 (C) Number of differential expressed genes (DEGs) between adjacent developmental  
209 stages. DEGs were defined by the threshold  $|\log_2(\text{Fold Change})| \geq 1$  and  $\text{FDR} \leq$   
210 0.05 by DESeq2.  
211 (D) Heatmap of expressed genes sorted by k-mean clustering across the samples  
212 collected at different developmental stages. The representative genes of each  
213 cluster are listed on the right.  
214 (E) Peak distribution of ATAC-seq and various histone modifications relative to genes.  
215 (F) PCA of ATAC-seq samples during spike development. Each dot represents one  
216 sample. Color represents different stages. Two bio-replicates were sequenced for  
217 each stage.  
218 (G) Chromatin accessibility dynamics in proximal regions (promoter and genic regions)  
219 during wheat spike development.  
220 (H-I) PCA of H3K27me3 (H) and H3K27ac (I) samples during spike development.  
221 Each dot represents one sample. Two bio-replicates were sequenced for each stage.  
222 (J) Gene expression, chromatin accessibility and H3K27me3 changes at representative  
223 genes during spike development. The y-axis indicates relative values of Z-scaled  
224 gene expression, chromatin accessibility and H3K27me3 levels.  
225

226 **A permissive chromatin environment facilitates vegetative-to-reproductive  
227 transition**

228 As indicated, chromatin accessibility increased globally during vegetative-to-  
229 reproductive transition at shoot apex (Figure 1G). We further look at differential  
230 accessible promoter regions (DAPR) from SAM to EL, SR, DR till SMI stages (Figure  
231 2A and Supplemental Table 4). In total, 49,153 DAPR was identified, categorized into  
232 6 clusters. Of them, majority of DAPR showed increased accessibility at either DR or  
233 SMI stages, including clusters 2,3,4,6 (Figure 2A and Supplemental Table 5).  
234 Interestingly, genes of those four clusters show higher positive correlation between  
235 chromatin accessibility and transcriptional dynamics ( $R > 0.5$ ) (Figure 2B). Indeed,  
236 genes with increased chromatin accessibility at DR or SMI stages is significantly  
237 overlapped with genes of elevated expression at DR or SMI as compared to SAM (1,920  
238 genes within gene set I; Figure 2C, Supplemental Figure 2A and Supplemental Table  
239 6). The degree of increased chromatin accessibility is highly correlated ( $R = 0.85$ ) with  
240 fold change of elevated expression level (Figure 2D). Gene Ontology (GO) term  
241 analysis suggests that hormone biosynthesis and signaling, inflorescence meristem

242 identity, asymmetric cell division are enriched in gene set I (Figure 2E). This highlights  
243 the synchronous between gain-of chromatin accessibility and elevated gene expression  
244 during vegetative apical meristem to inflorescence meristem transition (Figure 2F).

245

246 Besides, open chromatin could set a ‘primed’ status for gene activation later on (Bonifer  
247 et al., 2017; He and Li, 2018). There are 3,435 genes with gained chromatin  
248 accessibility at DR or SMI but elevated mRNA level at stages after SMI (Gene set II;  
249 Figure 2C, Supplemental Figure 2B and Supplemental Table 6). Those genes are mainly  
250 involved in hormones metabolism, floral organ identity, meristem development  
251 (Supplemental Figure 2C), which are important for spike formation similar as gene set  
252 I. By contrast, large amount of genes with gain-of chromatin accessibility but no change  
253 of mRNA level at tested spike developmental stages (Gene set III; Figure 2C and  
254 Supplemental Table 6), such as genes participated in polarity specification, cell size  
255 regulation, regulation of translation or protein transport (Supplemental Figure 2D).  
256 Thus, other chromatin features may also involve in the gene expression regulation of  
257 different gene sets.

258

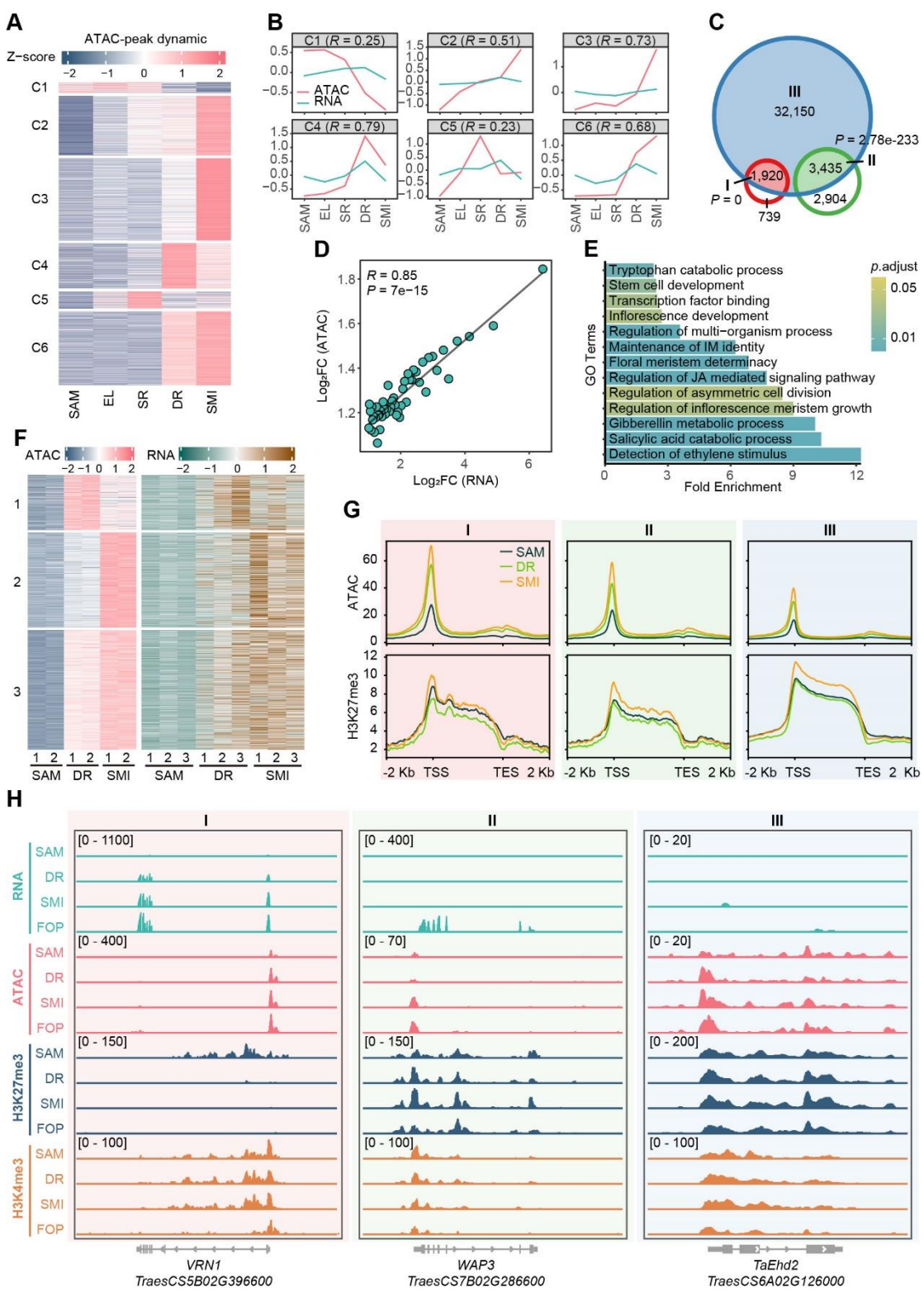
259 Indeed, H3K27me3 was closely related to transcriptional pattern of gene set I, II, III,  
260 while other histone modifications such as H3K27ac, H3K4me3, H2A.Z were not  
261 specifically correlated (Figure 2G and Supplemental Figure 2E). In details, genes in set  
262 I have relative higher chromatin accessibility at SAM stage, and sharply increased  
263 openness at DR and SMI stages, while reduced H3K27me3 level at DR as compared to  
264 SAM (Figure 2G). As example, well known flowering promoting gene *TaVRN-B1*  
265 shows increased chromatin accessibility and decreased H3K27me3 in genic region,  
266 while no change for H3K4me3 from SAM to DR and SMI stages (Figure 2H). Whereas  
267 for gene set II, though chromatin accessibility is elevated at SMI and GPD stages, but  
268 the relative openness is low. Meanwhile, H3K27me3 level doesn’t change from SAM  
269 to DR, even increased at SMI stage. The combined effect may result in the ‘primed’  
270 transcriptional status, which gene expression level increased later with the reduction of  
271 H3K27me3, such as *WAP3* (Figures 2G and 2H). For gene set III, lowest chromatin

272 accessibility gained and highest H3K27me3 coverage is observed, which can restrict  
273 gene activation (Figure 2G), as the case for *TaEhd2* gene (Figure 2H).

274

275 In summary, from vegetative to reproductive transition, the genome-wide chromatin  
276 accessibility increased and H3K27me3 reduced at selective part of genome that create  
277 a permissive environment for activation of inflorescence meristem genes and initial the  
278 reproductive development of shoot apex.

279



281 **Figure 2. Chromatin accessibility and H3K27me3 dynamics facilitate vegetative-  
282 to-reproductive transition of shoot apex.**

283 (A) K-means clustering of differential accessible promoter regions (DAPR) across the  
284 samples collected at stage from SAM to SMI.

285 (B) The chromatin accessibility and gene expression tendency for each cluster in A. R

286 value stands for the Pearson correlation coefficients.

287 (C) Overlap between genes with gained-chromatin accessibility of cluster 2, 3, 4, 6 in

288 (A) (blue circle), elevated expression at DR and SMI stage versus SAM stage (red

289 circle) and up-regulated at GPD, FMI, FOP stage versus former stages (green circle).

290 See also Supplemental Figures 2A and 2B. Geneset I showing overlap between red

291 and blue circle genes; geneset II showing overlap between red and green circle; while

292 rest genes from red circle belong to geneset III. Hypergeometric test was used to

293 calculate P-value for the enrichment of geneset I and II.

294 (D) Correlation of gene expression elevation (x-axis) and chromatin accessibility gain

295 (y-axis) from SAM to DR or SMI based on 1920 genes in geneset I in (C). Genes

296 were ranked by fold change of elevated expression and separated into 50 bins.

297 (E) GO enrichment analysis of 1920 genes in gene set I.

298 (F) Synchronous pattern of gene set I between the gain of chromatin accessibility and

299 elevation of gene expression from SAM to DR or SMI stage. Individual bio-replicate

300 are shown separately.

301 (G) Chromatin accessibility (top) and H3K27me3 (bottom) levels of genes in gene set

302 I, II, III at SAM, DR and SMI stages.

303 (H) IGV browser showing expression, chromatin accessibility and histone

304 modifications change at representative genes of *VRN1* (gene set I-left), *WAP3* (gene

305 set II-middle) and *TaEhd2* (gene set III-right).

306

### 307 **Gene co-expression and transcriptional regulatory network for spike architecture**

### 308 **formation**

309 Following the initiation of reproductive growth (DR), inflorescence undergoes several

310 processes, including SMI, GPD, FMI, and FOP to form the spike architecture (Figure

311 1A and Figure 3A). This is critical for determining SNS, contributing to grain yield.

312 We thus analyzed the genes co-expression and regulatory network to highlight the

313 potential factors that may govern the process.

314

315 We calculated the pseudo time of stages covering SMI to FOP based on PCA distance

316 (Figure 3A). GPD and FMI stages are close to each other, while distinct from SMI and

317 FOP. A total of 8,200 DEG was identified in the process of spike architecture formation

318 (any DEG among SMI, GPD, FMI, FOP), which could be clustered into 6 categories

319 (Figure 3B and Supplemental Table 7). Floral meristem determinacy and various

320 hormone metabolic genes are highly expressed at SMI; hormone signaling, polarity

321 establishment genes are active at GPD and FMI; while floral organ identity, polarity

322 specification genes are elevated at FOP (Figures 3B and 3C). Among those stage  
323 specific DEGs, we looked for enriched TFs. Within clusters 3 and 6, ERF and WRKY  
324 TFs are enriched and highly expressed at SMI stage. For GPD and FMI stages, NF-Y  
325 and SBP TFs are abundantly expressed within clusters 2 and 4. Whereas, MADS box  
326 TFs are outstanding at FOP stage of cluster 5 (Figures 3B and 3C). Such expression  
327 pattern fits well with the spatiotemporal switch of meristem identities in the context of  
328 hormone regulation (Kellogg, 2022; Koppolu et al., 2022), and indicates potential  
329 importance of individual TFs family in driving the transcriptional network that  
330 governing spike formation.

331

332 Accessible chromatin regions provide docking sites for TF binding. Binding motifs of  
333 AP2/ERF, bHLH and SPL showed greatest accessibility variability during SMI to FOP  
334 (Figure 3D), suggesting the potential importance of those TFs. Based on the TF-motif  
335 recognition pairs, in combination with the co-expression pattern of TFs and  
336 downstream targets, we are able to construct a hierarchy TRN by integrating the multi-  
337 stages ATAC-seq and RNA-seq data (Supplemental Figure 3A). Totally, 36,908 pairs  
338 of TFs-target genes interactions were identified, covering a total of 5,106 genes, of  
339 which 4,916 pairs were regulated between TFs (Supplemental Figure 3B). A clear  
340 sequential regulatory relation among time-serial expressed gene clusters from SMI to  
341 FMI is observed as C6-C3-C2-C4 (Figure 3E). Whereas, FOP specific expressed genes  
342 in C1 and C5 are separated and regulated each other (Figure 3E), indicating different  
343 transcriptional regulatory networks between spikelet and floret development. TFs of  
344 ERF, B3, TCP, DOF and MIKC-MADS may play core regulatory role in this network  
345 as more targets being identified (Figure 3F and Supplemental Figure 3C). Some  
346 functionally characterized factors that involved in wheat spike development can be  
347 found in the network, such as *TaTB1* (Dixon et al., 2018), *VRN1* (Li et al., 2019),  
348 *TaFUL3* (Li et al., 2019) (Figure 3G), indicating the capability of our TRN in capturing  
349 important regulators.

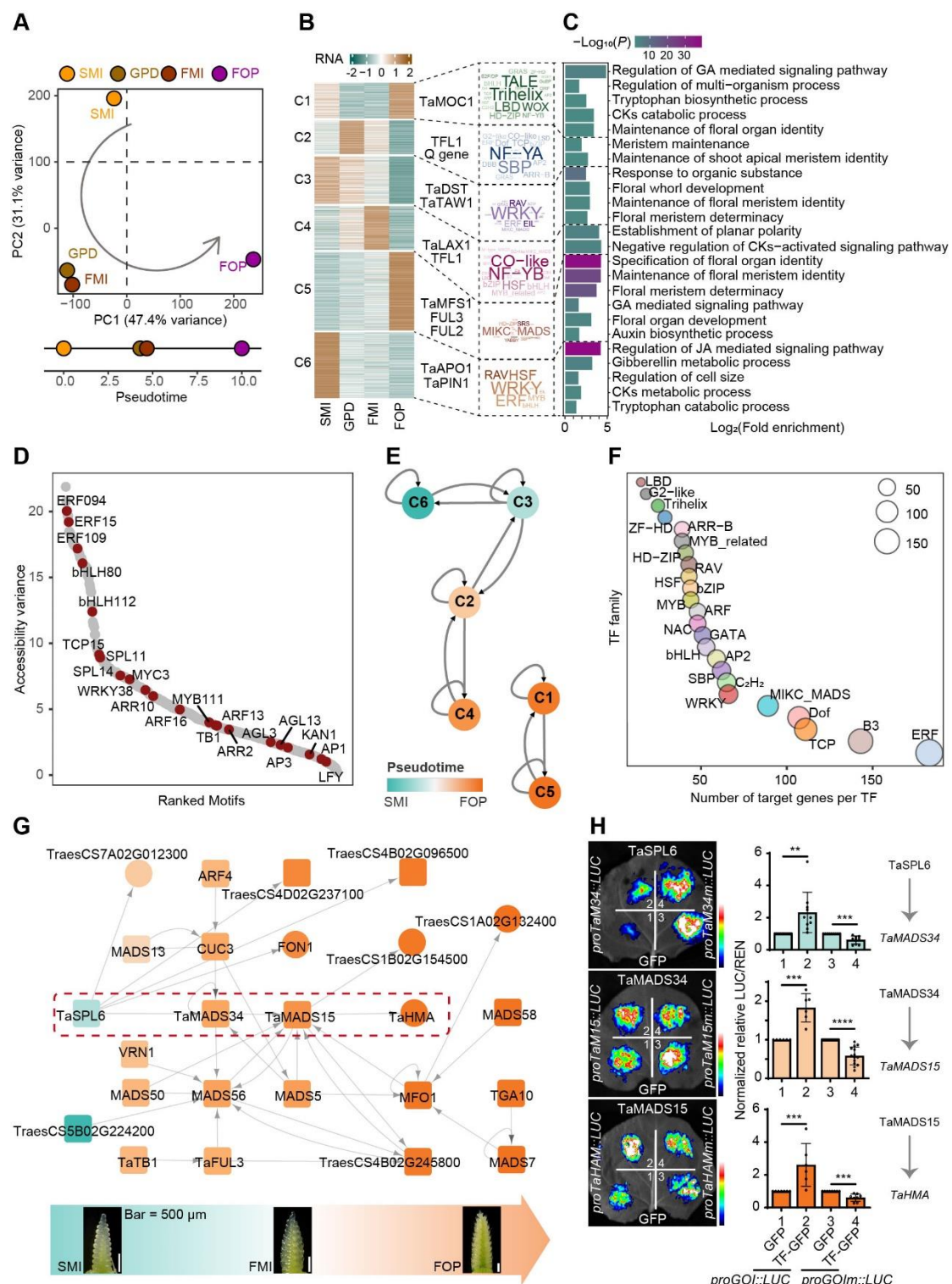
350

351 To validate the prediction power of the hierarchy of transcriptional regulation among  
352 TFs, we extract a small module that contains factors being functionally studied  
353 individually in other crops but without known of regulatory relations, such as *SPL6*  
354 (Wang et al., 2018), *MADS34* (Lin et al., 2014; Meng et al., 2017; Zhu et al., 2022),  
355 *MADS15* (Wang et al., 2010; Wu et al., 2017) (Figure 3G). From their temporally  
356 expression pattern (Supplemental Figure 3D) and the presence of specific motifs in the  
357 open chromatin of each gene (Supplemental Figure 3E), we speculate a positive  
358 transcriptional regulation hierarchy following *SPL6-MADS34-MADS15-HMA*  
359 module. Indeed, we observed a positive transcriptional regulatory circuit among them  
360 by using luciferase reporter assay in tobacco leaves (Figure 3H and Supplemental  
361 Figure 3F). As well, such regulation circuit is dependent on the TF-motif specific  
362 recognition (Figure 3H and Supplemental Figure 3F).

363

364 Thus, the TRN constructed could well predict the potential important regulatory factors  
365 and their transcriptional regulatory relationships during the process of spike  
366 development.

367



368

369 **Figure 3. Transcriptional regulatory network (TRN) governing spike architecture  
370 formation.**

371 (A) Principal-components plots of gene expression from SMI to FOP stages. The  
372 developmental time units (DTU) values calculated based on scaled straight  
373 distance between two adjacent stages was shown in the lower panel.

374 (B) K-mean clustering of DEGs from SMI to FOP stage and representative genes in

- 375 each cluster.
- 376 (C) TF family enrichment and GO enrichment analysis within each cluster in B.
- 377 (D) Motif accessibility variance from SMI to FOP stage.
- 378 (E) Hierarchical transcriptional regulations of sequentially expressed gene clusters
- 379 from (B). *P*-value was determined by the hypergeometric test.
- 380 (F) Average target genes number of each TF family in the TRN. The size of dot
- 381 represents number of target genes.
- 382 (G) TRN for represented key TFs participated in spike development, from SMI to FOP
- 383 stages. Genes were roughly ranked by the expression timing from left to right as
- 384 indicated by different colors gradients. TFs and non-TF coding target genes were
- 385 in solid rectangle or circle, respectively. The dashed red rectangle frame indicates
- 386 a four-layer regulation module tested in (H).
- 387 (H) Luciferase reporter assays validation of transcriptional regulation among
- 388 representative TF-target pairs as indicated. Mutations of the TF binding sites were
- 389 introduced in the promoter region of target genes separately. Student's *t* test was
- 390 used for the statistical significance (\*\*,  $p \leq 0.01$ ; \*\*\*,  $p \leq 0.001$ ).
- 391

392 **Integration of multi-data to systematically screen regulators shaping spike**

393 **development**

394 The open region of chromatin is crucial for the establishment of transcriptional

395 regulatory relationships (Klemm et al., 2019). Indeed, more binding motifs of TFs are

396 significantly present in the open region of chromatin (Figure 4A), with lower DNA

397 variation at the TFs binding footprints (Figure 4B) (Zhou et al., 2020). Furthermore,

398 the open chromatin regions contain significantly higher GWAS signals with related to

399 spike morphology traits from previous publication (Figure 4C and Supplemental Table

400 8). The QTL frequency of open chromatin regions quintupling that of the whole genome

401 totally, with analogical results obtained for concrete spike related traits, such as spike

402 length (SL), SNS, GNPS (Figure 4D). Take the fertile spikelet number per spike (FSPS)

403 as an example, a total of 153 SNPs passed the significance threshold from GWAS

404 analysis and considered as significant associated loci (Figure 4F and Supplemental

405 Table 9). We enlarged the candidate region to 1 Mb centered on the GWAS signal peak,

406 2,916 genes were identified as candidate genes. Among the 2,916 genes, 1762 genes

407 (60.43%, C1 and C4) present the highest openness of chromatin accessibility at DR or

408 SMI, when spikelet primordia were undergoing initiation/ differentiation and

409 considered to be critical for determination of final SNS (Figure 4E and Supplemental

410 Figure 4A). In addition, 438 genes (15.02%, C6) exhibit to most open at FMI, which is  
411 crucial to the floret development and seed setting (Supplemental Table 9). Analogical  
412 results were observed for SL, spikelet density (SD), and SNS (Supplemental Figure  
413 4B). This result indicated that large proportion of GWAS candidate genes possess high  
414 chromatin openness at key developmental stage relating to the corresponding trait.

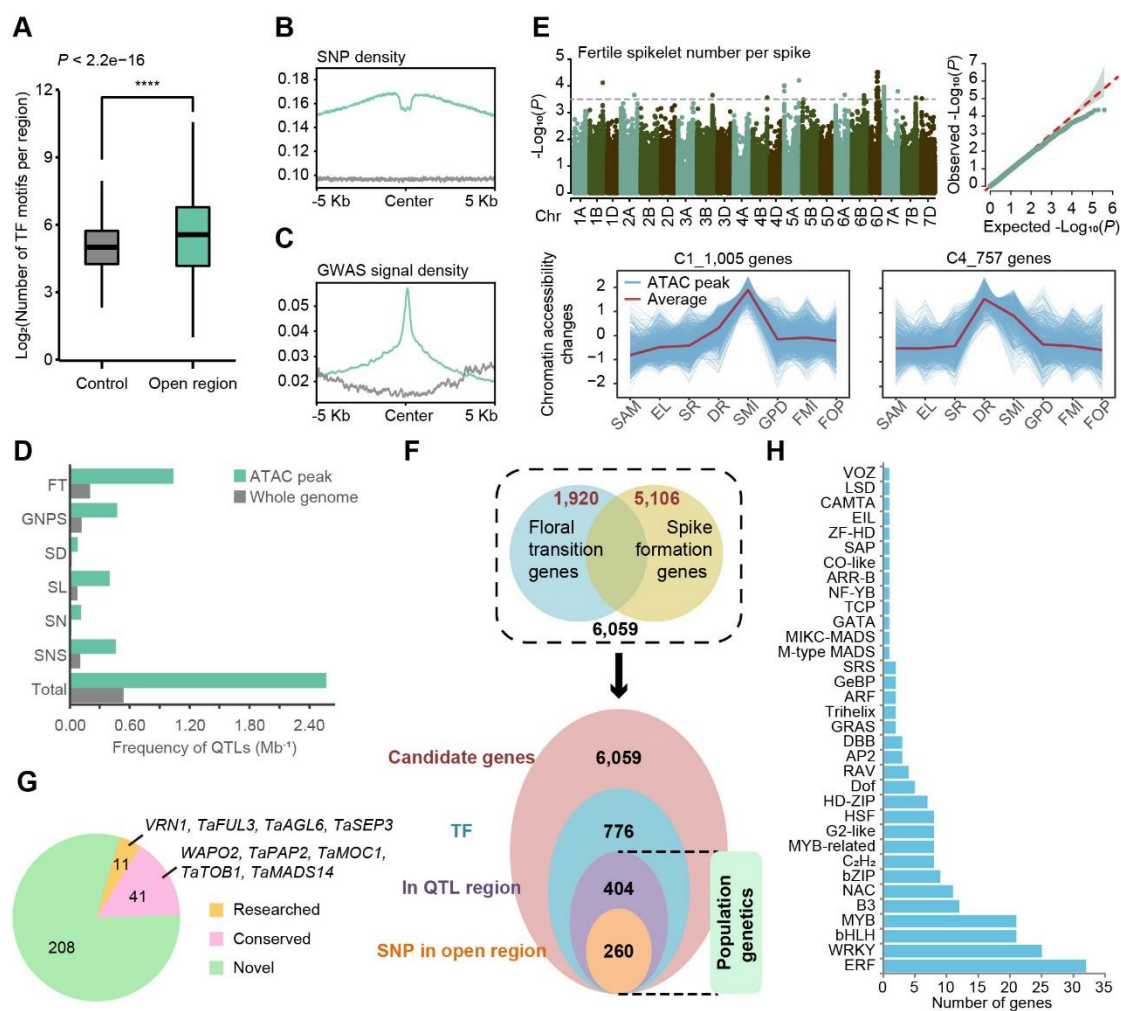
415

416 We further integrate the spike traits-associated genetic regions from population genetics  
417 study (Supplemental Table 8) with key regulators identified for floral transition, giving  
418 the importance of regulating duration of inflorescence meristem development (Boden  
419 *et al.*, 2015; Finnegan *et al.*, 2018), as well as the regulators in the TRN network that  
420 potentially governing the formation of spike (Figure 4F). With focusing on TFs coding  
421 genes, we got 776 candidates for further screening (Figure 4F and Supplemental Table  
422 10). Among them, more than half (404 TFs) are within the spike morphological traits-  
423 associated genetic regions (Figure 4F and Supplemental Table 10). We further narrow-  
424 down the candidates to 260 TFs by looking for presence of SNP in the open chromatin  
425 region of those TFs (Figure 4F and Supplemental Table 10), which is likely to affect  
426 the transcriptional regulatory circuit and rewire the TRN of spike development.

427

428 Of the candidate TFs, we categorize them into three classes, termed as ‘researched’ for  
429 functional studied in wheat and ‘conserved’ as orthologue being studied in other species  
430 as well as ‘novel’ for functional unknown for wheat and other crops (Figure 4G).  
431 Among the 260 TFs, 11 factors are ‘researched’ in wheat, including *VRN1* (Li *et al.*,  
432 2019), *TaFUL3* (Li *et al.*, 2019), *TaAGL6* (Kong *et al.*, 2022), *TaSEP3* (Zhang *et al.*,  
433 2021). Another 41 factors are ‘conserved’, including *MOC1* (Zhang *et al.*, 2015), *PAP2*  
434 (Kobayashi *et al.*, 2010; Kobayashi *et al.*, 2012), *MADS14* (Wu *et al.*, 2017), etc. (Figure  
435 4G and Supplemental Table 11). Of note, majority of candidates identified are ‘novel’  
436 TFs, as many as 208, without study in wheat or other crops. These TFs are enriched in  
437 ERF, WRKY, bHLH, MYB, B3 families (Figure 4H and Supplemental Table 11). Thus,  
438 by integrating of multi-dimensional data, we have identified potential key regulators  
439 for spike development.

440



441

442 **Figure 4. Screening for key TFs in spike development by integration of multi-**  
443 **dimensional data.**

- 444 (A-C) Enrichment of TF binding motifs (A), SNP density (B) and GWAS signals of  
445 multi-trait (C) in open chromatin regions. Green and gray refer to open chromatin  
446 regions and control regions, respectively.
- 447 (D) The QTL frequency of spike morphology related traits in open chromatin regions  
448 (light green bar) and whole genome (gray bar). The QTL frequency of each trait  
449 were determined with QTL numbers divided by physical length of the open  
450 chromatin regions and whole genome, respectively.
- 451 (E) The chromatin openness patterns of fertile spikelet number per spike (FSPS) trait  
452 correlated candidate genes. Manhattan plot (up-left) and Quantile-Quantile plot  
453 (up-right) showing the significant associated signals of FSPS using a mixed linear  
454 model (MLM). The chromatin accessibility change showed GWAS signal  
455 associated genes specifically open at DR and SMI (low), with average trends  
456 highlighted in red. The y-axis represents z-scaled chromatin accessibility across  
457 developmental stages.
- 458 (F) Schematic of the strategy used for key factors identification for shaping spike

459                   architecture.  
460 (G) Pie chart summary of candidate factors for spike development in each category as  
461                   indicated. Represented genes' name were listed.  
462 (H) Gene number of corresponding TF families for the 208 potential novel TFs  
463                   governing spike development.

464

465 **Validation of the genetic regulatory hierarchy of 'conserved' factors for spike  
466 development**

467 Among the 'conserved' factors, we again found *TaSPL6*, *TaMADS34*, *TaMADS15*  
468 (Figure 4G), as showing up in the TRN governing spike development (Figures 3G and  
469 3H). Thus, we wonder whether these factors are indeed involved in shaping spike  
470 architecture in wheat.

471

472 *In situ* hybridization finely characterize the spatial-temporal expression profile of these  
473 factors (Figure 5A). *TaSPL6* was weakly expressed in the SAM, fixedly expressed in  
474 the IM tip, spikelet primordia and floret meristem. *TaMADS34* and *TaMADS15* were  
475 both expressed throughout the SAM, SMI and FOD stages and highly expressed in the  
476 spikelet and floral primordia. *TaHMA*, a downstream target of *TaMADS15*, also  
477 expressed in the spikelet and floral primordia. Similar spatiotemporal expression  
478 pattern supports their transcriptional regulatory hierarchy and potential role in spikelet  
479 or floret development. Furthermore, we generate RNAi transgenic wheat of *TaSPL6*,  
480 *TaMADS34* and *TaMADS15*, respectively (Supplemental Figure 5A). As expected,  
481 *TaMADS34-RNAi* and *TaMADS15-RNAi* plants exhibit similar phenotypes, with  
482 shorter SL, decreased SNS and GNPS (Figures 5B-5D and Supplemental Figure 5B).  
483 *TaSPL6-RNAi* plants also show altered spike developmental phenotype, but with longer  
484 SL, increased SNS and GNPS (Figures 5B-5D and Supplemental Figure 5B). This is  
485 likely because that *TaSPL6* is on the top layer of hierarchy TRN, it can regulate multi-  
486 targets in addition to *TaMADS34* (Figure 3G). Consistent with the LUC reporter assay  
487 *in vitro* (Figure 3H), in *TaSPL6-RNAi* transgenic wheat, we observed significant  
488 reduced expression of *TaMADS34* (Figure 5E), further indicating that *TaSPL6*  
489 positively regulate *TaMADS34*. Similar expression pattern was observed for supporting

490 that TaMADS34 activated *TaMADS15*, and TaMADS15 promoted *TaHMA* (Figure  
491 5E). Therefore, the spike developmental defects of TF-RNAi lines, similar  
492 spatiotemporal expression pattern and relative genes expression level in transgenic  
493 wheat prove that TaSPL6-TaMADS34-TaMADS15-*TaHMA* functions as a regulatory  
494 module during wheat spike development.

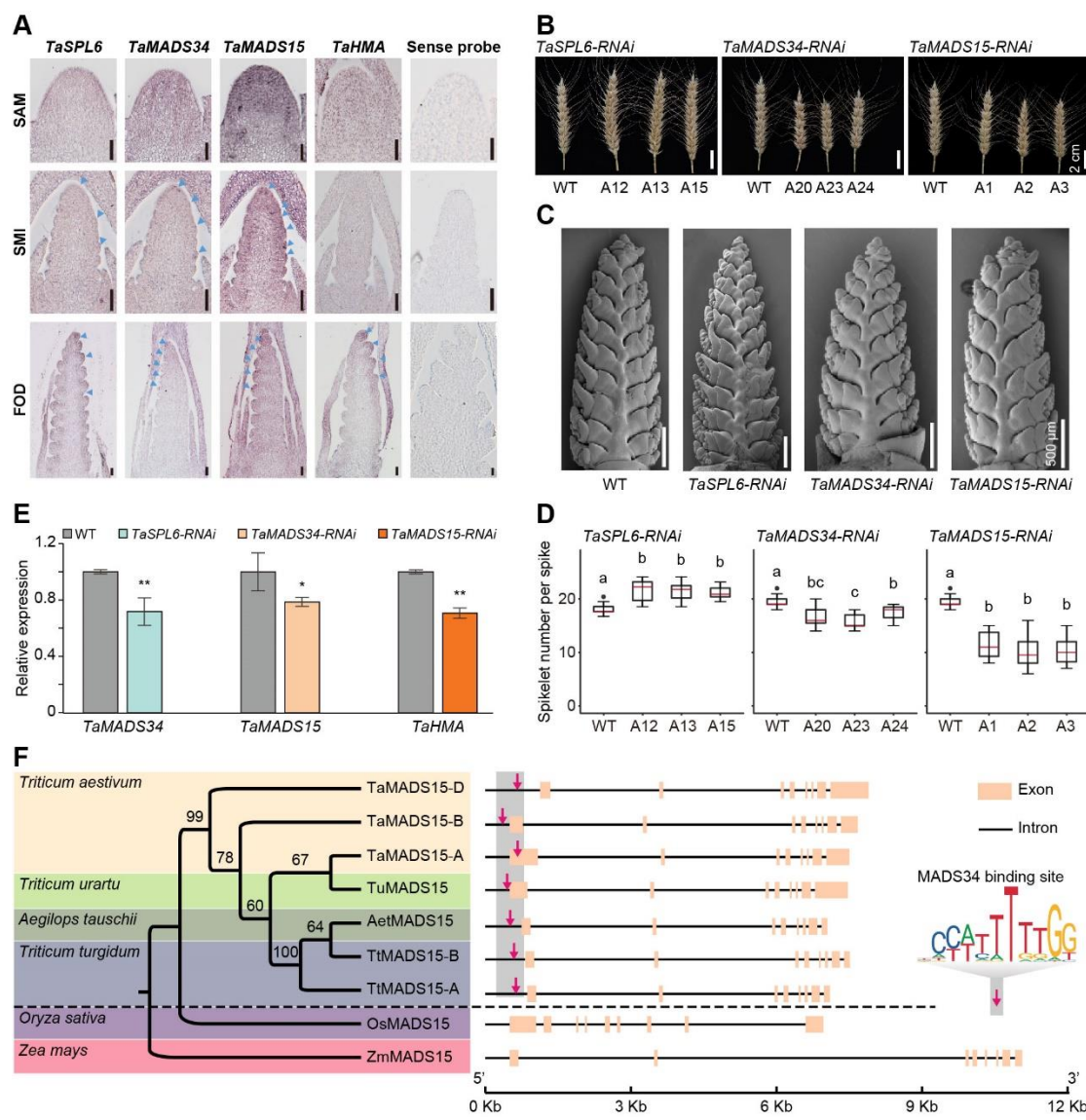
495

496 We further analyzed the conservation of this hierarchy regulatory module among  
497 TaSPL6-TaMADS34-TaMADS15-*TaHMA* in *Triticum* and *Gramineae* from an  
498 evolutionary perspective (Figure 5F). In diploid wheat AA, DD, tetraploid wheat  
499 AABB, and hexaploid wheat AABBDD, there is a MADS34 binding motif  
500 (CCATTTTG) in the similar promoter region of the *MADS15* homologous genes  
501 (Figure 5F). Similarly, in the promoter region of *MADS34* homologous genes, the  
502 binding motif of SPL6 (CCGTACGG) exists (Supplemental Figure 5C). This indicates  
503 that this regulatory module may be conserved within *Triticum*. However, in rice (*Oryza*  
504 *sativa*) or Maize (*Zea mays*), the promoter region of *MADS15* lacks the MADS34  
505 binding motif, the promoter region of *MADS34* lacks the SPL6 binding motif,  
506 indicating that this regulatory module may be differentiated in grasses (Figure 5F and  
507 Supplemental Figure 5C).

508

509 Thus, the ‘conserved’ factors we identified were indeed involved in regulating spike  
510 development in wheat, and the hierarchy transcriptional regulatory circuit is likely  
511 maintained within *Triticum* tribe.

512



513

514 **Figure 5. SPL6-MADS34-MADS15-HMA module regulates spike development in**  
 515 **wheat.**

- 516 (A) Spatiotemporal expression patterns of *TaSPL6*, *TaMADS34*, *TaMADS15* and  
 517 *TaHMA* at different spike developmental stages, as indicated by *in situ*  
 518 hybridization. Sense probe is used as negative control. Scale bars = 100 µm.
- 519 (B) Spike developmental defects of T2 RNAi transgenic plants of *TaSPL6*, *TaMADS34*,  
 520 *TaMADS15* as compared to wild-type (WT) Fielder. Scale bars=2 cm.
- 521 (C) Scanning electron micrographs (SEM) of young spikes from WT and RNAi  
 522 transgenic plants of *TaSPL6*, *TaMADS34*, *TaMADS15* at DR, GPD and FOP stages.  
 523 Scale bars = 500 µm.
- 524 (D) Quantification of spikelet number per spike (SNS) between WT, *TaSPL6-RNAi*,  
 525 *TaMADS34-RNAi* and *TaMADS15-RNAi* transgenic plants. Two-tailed Student's t-  
 526 tests. In box plots, the box limits indicate the 25th and 75th percentiles, the  
 527 whiskers indicate the full range of the data, and the centre line indicates the  
 528 median. Different letters mean significant difference at  $p < 0.01$ .

- 529 (E) The expression level of *TaMADS34*, *TaMADS14*, *TaHMA* in WT or *TaSPL6-RNAi*,  
530 *TaMADS34-RNAi*, *TaMADS15-RNAi* transgenic plants. Expression level of genes  
531 in WT is set as 1.0, the relative expression of each gene in RNAi plants is shown  
532 as average  $\pm$  SD of three replicates. Student's *t* test was used for the statistical  
533 significance (\*,  $p \leq 0.05$ ; \*\*,  $p \leq 0.01$ ).  
534 (F) The conservation of TaMADS34 binding motif (CCATTTTG) at chromatin  
535 accessible region of *MADS15* orthologs in different *Triticum*, but not *Oryza sativa*  
536 or *Zea mays*. Phylogenetic tree of corresponding species is indicated on the left.  
537 Schematic diagram of gene structure and presence or absence of MADS34 binding  
538 CArG motif sites is shown on the right.

539

540 **Verification of novel regulators for spike development**

541 To evaluate our strategy of identifying novel regulators for wheat spike development,  
542 we investigated the spike developmental defects of meta TILLING mutant lines in  
543 Kronos (Krasileva et al., 2017; Uauy et al., 2009), Cadenza (Krasileva et al., 2017) and  
544 KN9204 (we generated and did exome sequenced, unpublished), of which the mutated  
545 sites were identified by whole exome sequencing.

546

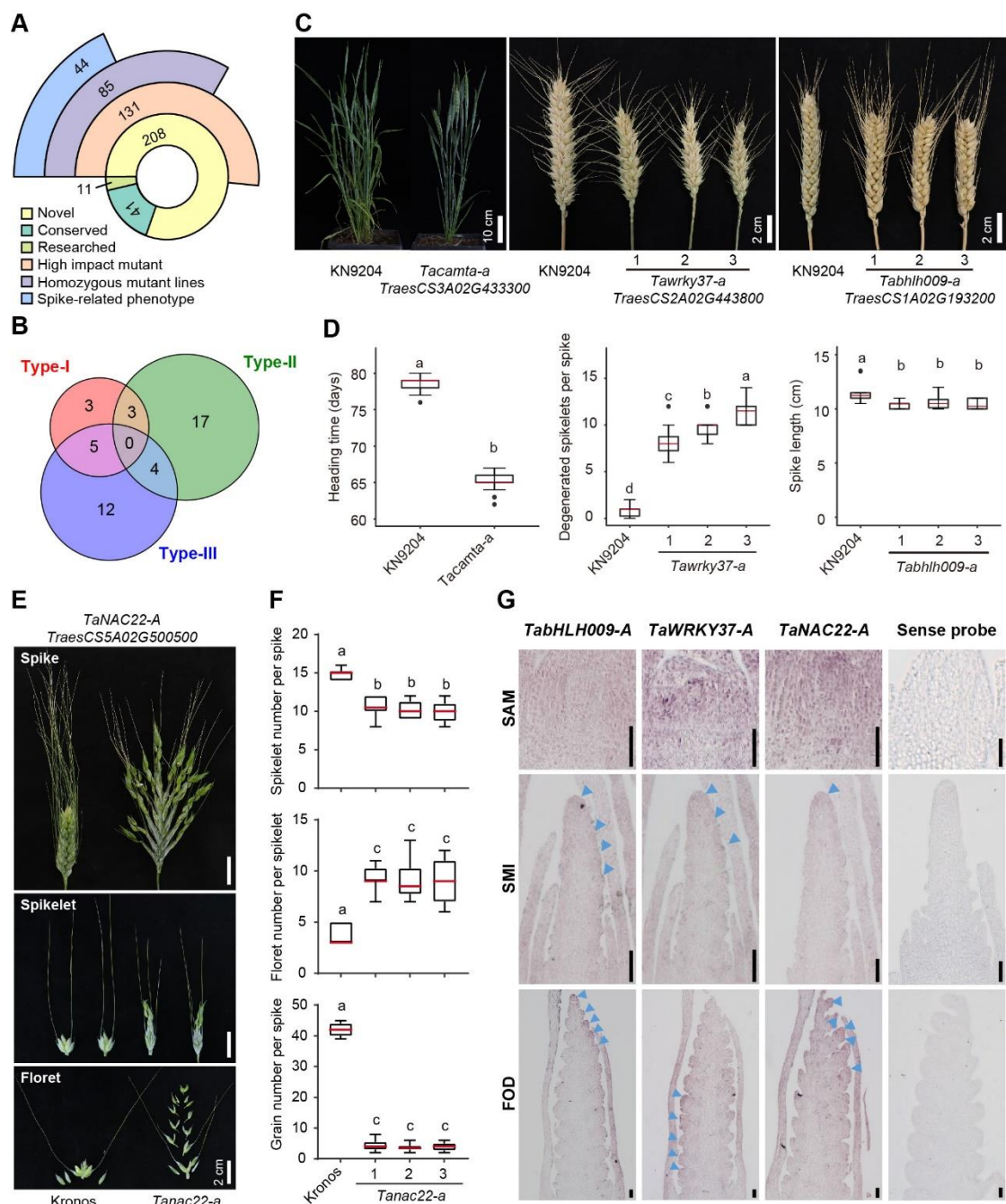
547 Of the 208 novel TFs, 131 TFs were found to have at least one mutant line that  
548 containing loss-of-function mutation (Figure 6A and Supplemental Table 11). Among  
549 the 85 TFs with homozygous TILLING mutant lines, 44 TFs (51.76%) exhibited spike  
550 developmental defects within three major types, including flowering time difference  
551 (Type I,  $n=11$ ), degeneration of spikelet or floret (Type II,  $n=24$ ), and altered SL or  
552 SNS (Type III,  $n=21$ ) (Figure 6B and Supplemental Table 11). Representative mutant  
553 lines of different types were shown (Figures 6C and 6E and Supplemental Figure 6).  
554 For instance, *TraesCS3A02G433300* (*TaCAMTA-A*) mutant showed an early flowering  
555 phenotype with about 2 weeks earlier than the control line; *TraesCS2A02G443800*  
556 (*TaWRKY37-A*) mutant showed more degenerated spikelet number per spike (DSNS)  
557 at basal part of inflorescence, resulted in decreased SNS/GNPS; *TraesCS1A02G193200*  
558 (*TabHLH009-A*) mutant showed reduced spike length and increased spikelet density  
559 (Figures 6B-6D and Supplemental Figure 6A). The similar phenotype of *TaWRKY37-*  
560 *A* and *TabHLH009-A* genes also exhibit in the Cadenza mutant (Supplemental Figures  
561 6B and 6C). The loss-of-function mutant of *TraesCS5A02G500500* (*TaNAC22-A*) in

562 the tetraploid wheat Kronos (*Triticum turgidum*) exhibits increased floret number per  
563 spikelet (about 10 florets in a spikelet) due to non-terminated floral primordium  
564 differentiation, and most of the florets were abortive which result in decreased GNPS  
565 (Figures 6E and 6F). We further confirmed the spatiotemporal expression pattern of  
566 those genes by *in situ* hybridization (Figure 6G). Consistent with their morphologic  
567 defects, *TaWRKY37-A*, *TabHLH009-A* and *TaNAC22-A* genes are all expressed at the  
568 spikelet initiation region and the spikelet/floral primordia; while *TaWRKY37-A* is  
569 highly expressed in the IM tip and the spikelet and floral meristem at the base of spike,  
570 *TabHLH009-A* is highly expressed in the spikelet and floral meristem at the upper  
571 region of spike, and *TaNAC22-A* has significant expression in the SAM and floral  
572 primordia (Figure 6G).

573

574 Taking the advantage of available TILLING mutant lines, we have proved that novel  
575 TFs identified by our integration strategy played important role in regulating spike  
576 development. The strategy used for screening novel factors is efficient and the  
577 identified factors were worth for in-depth study.

578



579

580 **Figure 6. Novel factors identified regulate spike development.**

- 581 (A) Summary of novel TFs with different categories of KN9204 TILLING mutant lines.
- 582 (B) Venn-diagram of different type of spike-related phenotype presented in KN9204
- 583 TILLING mutant lines containing homozygous mutation at novel TFs coding
- 584 genes.
- 585 (C) Represented KN9204 TILLING mutant lines of type I/II/III spike developmental
- 586 defects as compared to control KN9204. Type I, CAMTA (*TraesCS3A02G433300*,
- 587 *Tacamta-a*), Scale bar = 10 cm; type II, WRKY (*TraesCS2A02G443800*,
- 588 *Tawrky37-a*), Scale bar = 2 cm; type III, bHLH (*TraesCS1A02G193200*,
- 589 *Tabhlh009-a*), Scale bars = 2 cm.

- 590 (D) Quantification of different types of spike developmental defects in represented  
591 KN9204 TILLING mutant lines, as heading date of *Tacamta-a*, degenerated  
592 spikelet number per spike (DSNP) of *Tawrky37-a*, spikelet density of *Tabhlh009-a*,  
593 the Wild-type is KN9204. Two-tailed Student's *t*-tests. Different letters mean  
594 significant difference at  $p < 0.01$ .
- 595 (E) The spike developmental defect of *TraesCS5A02G500500* (*TaNAC22-A*) mutant  
596 lines as compared to control Kronos. Scale bars = 2 cm.
- 597 (F) Quantification of floret number per spikelet (FNPS), gain number per spike  
598 (GNPS), spikelet number per spike (SNS) for represented Kronos TILLING  
599 mutant lines containing mutation of *TraesCS5A02G500500* (*Tanac22-a*). Two-  
600 tailed Student's *t*-tests. In box plots, the box limits indicate the 25th and 75th  
601 percentiles, the whiskers indicate the full range of the data, and the centre line  
602 indicates the median. Different letters mean significant difference at  $p < 0.01$ .
- 603 (G) Spatiotemporal expression patterns of *TaWRKY37-A*, *TabHLH009-A* and  
604 *TaNAC22-A* at different spike developmental stages, as indicated by *in situ*  
605 hybridization. Sense probe is used as negative control. Scale bars = 100  $\mu$ m.

606

607 **Regulation of wheat spike architecture by novel factor TaMYB4-A**

608 To further explore the potential application of integrated TRN and GWAS analysis in  
609 dissecting molecular function of individual gene in wheat spike development, we took  
610 a novel regulator TaMYB4-A for in-depth study.

611

612 *TraesCS6A02G224200* (TaMYB4-A) was one of the TFs from the TRN (Supplemental  
613 Figure 3B). It also located within a genetic region that was significantly associated with  
614 FSPS by GWAS analysis (Figure 7A and Figure 4F). Two haplotypes (C-type Vs T-  
615 type) of *TaMYB4-A* could separate a natural population of 214 wheat varieties with  
616 significant differences in FSPS (Figure 7B). Consistently, we find *TaMYB4-A* is  
617 initially expressed in the spikelet initiation region at DR stage, and highly expressed in  
618 the spikelet and floral primordia during SMI and FMI stages by *in situ* hybridization  
619 (Figure 7C), which fits its role in determining spikelet number and. Further, we  
620 obtained loss-of-function mutant lines of *TaMYB4-A* from KN9204 and Cadenza  
621 TILLING libraries (Figure 7D and Supplemental Figure 7A). Mutation of *TaMYB4-A*  
622 significantly reduced SL, SNS, GNPS (Figures 7D and 7E and Supplemental Figures  
623 7B and 7C), which further confirmed its function in regulating spikelet development.

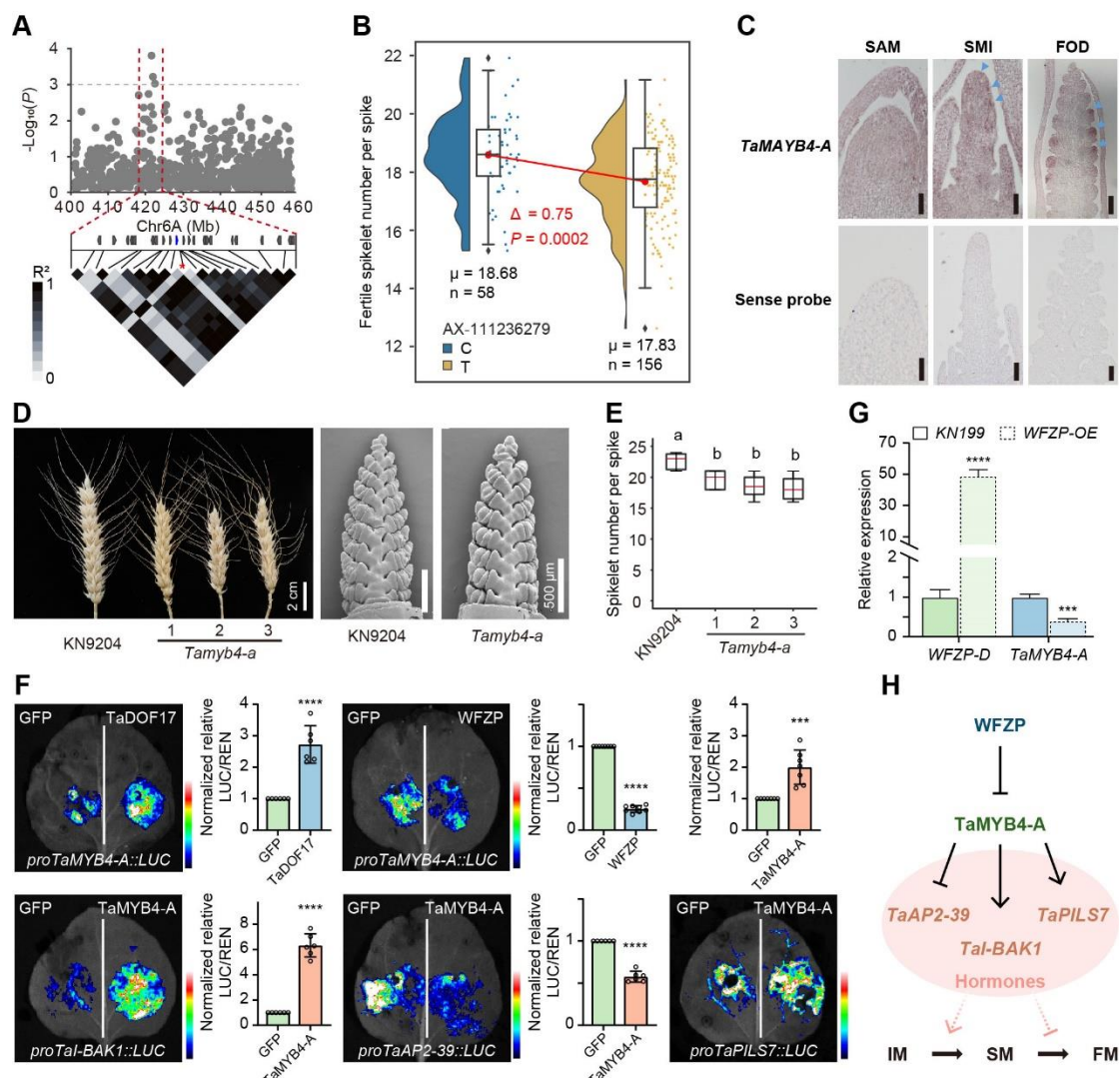
624

625 We further study the molecular regulation network of *TaMYB4-A* in mediating spike  
626 development. Based on the TRN generated, we extract the hierarchy transcription  
627 regulatory module containing *TaMYB4-A* (Supplemental Figure 7D). Among the  
628 potential upstream regulators of *TaMYB4-A*, we further confirmed that WFZP and a  
629 DOF type TF *TaDOF17* (*TraesCS2B02G592700*) could repress or active *TaMYB4-A*  
630 in the reporter assay in tobacco leaves, respectively (Figure 7F and Supplemental Figure  
631 7E). This also fits with the temporal expression pattern of *WFZP*, *TaDOF17* and  
632 *TaMYB4-A* during spike formation process. *TaDOF17* and *TaMYB4-A* showed similar  
633 pattern but *TaDOF17* changed ahead of *TaMYB4-A*, whereas *WFZP* elevated after SMI  
634 with *TaMYB4-A* reduction after SMI stage (Supplemental Figure 7F). WFZP repression  
635 of *TaMYB4-A* is further evidenced by down regulation of *TaMYB4-A* in WFZP gain-of  
636 function transgenic wheat (Figure 7G) (Li et al., 2021). Among the numerous potential  
637 downstream targets of *TaMYB4-A* (Supplemental Figure 7D), several genes were  
638 confirmed to be regulated by *TaMYB4-A* in reporter assay in tobacco leaves (Figure  
639 7F). This includes *TaAP2-39* (*TraesCS2D02G425700*), of which homologous being  
640 proved to regulate the development of tiller and panicle/inflorescence by controlling  
641 the balance of ABA/GA in rice (Yaish et al., 2010), and *TaI-BAK1*  
642 (*TraesCS7D02G416900*), with homologous encoding a Brassinosteroid insensitive 1-  
643 associated kinase 1, reported to increase panicle length and grain number per panicle  
644 when overexpressed in rice (Khew et al., 2015), as well as *TaPILS7*  
645 (*TraesCS5A02G354300*), encoding an auxin efflux carrier component (Figure 7F).  
646 Consistently, *TaAP2-39*, *TaI-BAK1* and *TaPILS7* showed a synchronized temporal  
647 expression pattern as *TaMYB4-A* during spike formation process (Supplemental Figure  
648 7F).

649

650 Thus, *TaMYB4-A* positively regulates fertile spikelet likely through regulating  
651 hormones homeostasis and/or signaling, acting downstream of and repressed by WFZP  
652 (Figure 7H).

653



654

655 **Figure 7. The novel factor TaMYB4-A regulates spike architecture.**

- 656 (A) *TaMYB4-A* located in a GWAS signal associated with FS<sub>PS</sub>. A manhattan  
657 locuszoom were plot with gene models and linkage disequilibrium plot of SNPs  
658 shown below, in 5-Mb physical scale centered on the peak SNP.
- 659 (B) FS<sub>PS</sub> distribution between haplotypes (C and T) defined by the peak SNP. The bars  
660 within raincloud box plots represent 25th percentiles (haplotype T), medians, and  
661 75th percentiles (haplotype C). Mean values of two haplotypes were linked by a  
662 red line, and one-way ANOVA was used to determine significant differences.
- 663 (C) Spatiotemporal expression pattern of *TaMYB4-A* is indicated by *in situ*  
664 hybridization. Scale bars = 100  $\mu$ m.
- 665 (D) The spike phenotype and scanning electron micrographs (SEM) of *TaMYB4-A*  
666 (*TraesCS6A02G224200*) mutant from the KN9204 TILLING mutant library. Scale  
667 bars = 2 cm (left), 500  $\mu$ m (right).
- 668 (E) Statistics comparison of spikelet number per spike (SNS) between KN9204 and  
669 *Tamyb4-a* mutant lines. Two-tailed Student's *t*-tests. In box plots, the box limits  
670 indicate the 25th and 75th percentiles, the whiskers indicate the full range of the  
671 data, and the centre line indicates the median. Different letters mean significant  
672 difference at  $p < 0.01$ .

673 (F) Luciferase reporter assays of *TaMYB4-A* regulatory network. Schematic diagram in  
674 the left part showing the vectors used in this array. Student's *t*-test was used for  
675 the statistical significance. \*\*,  $p < 0.001$ ; \*\*\*\*,  $p < 0.0001$ .  
676 (G) The expression level of *WFZP* and *TaMYB4-A* in KN199, *WFZP*-OE transgenic  
677 plants by RT-qPCR. The error bars denote  $\pm$ SD. \*\*,  $p \leq 0.001$ ; \*\*\*\*,  $p \leq 0.0001$ .  
678 (H) The working model representing the possible function and genetic network of  
679 *TaMYB4-A* in wheat.

680

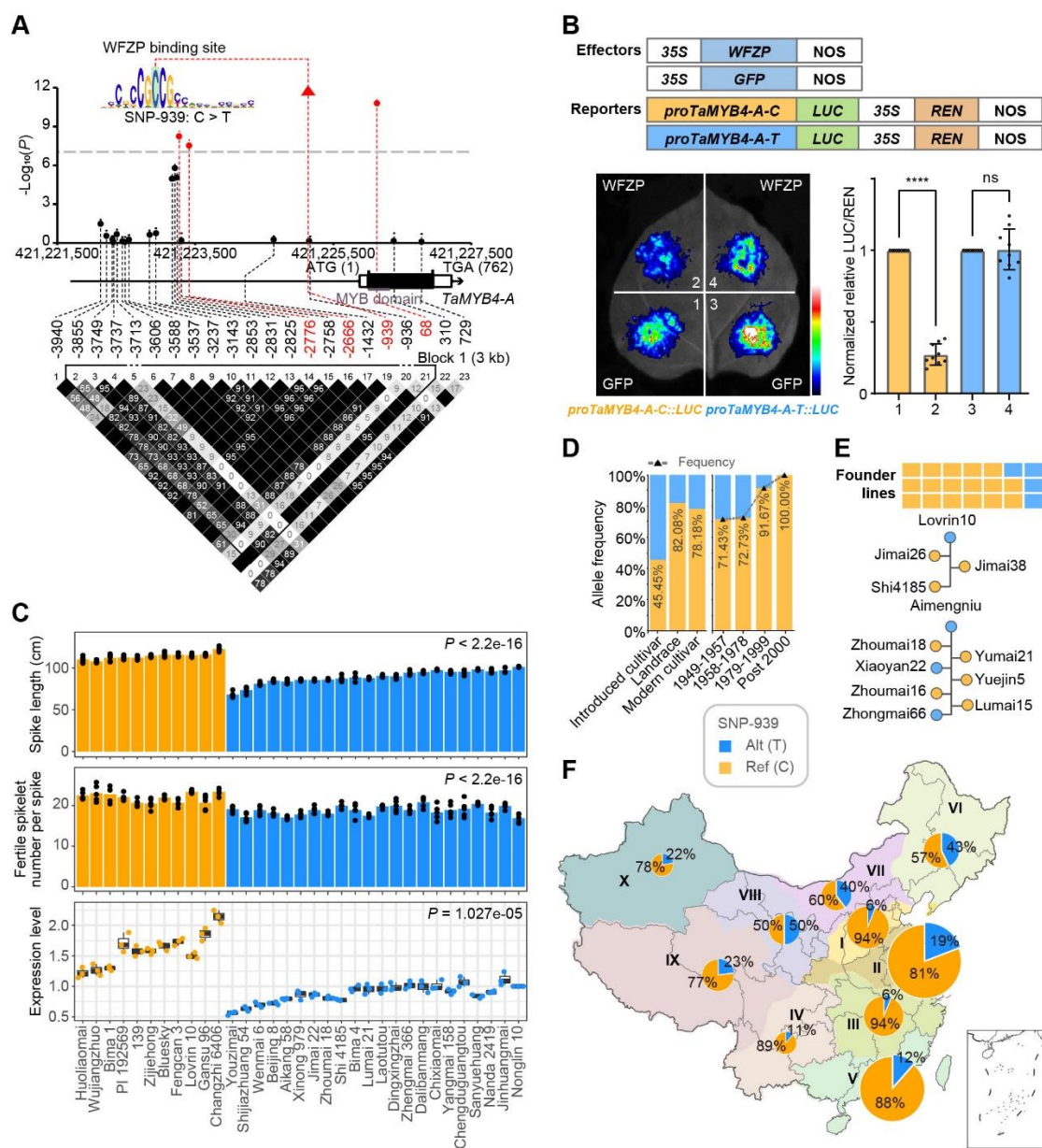
681 **SNP at WFZP binding site within *TaMYB4-A* promoter mediates spike  
682 architecture selection during breeding process in China**

683 Next, we wonder how the different haplotypes of *TaMYB4-A* could affect its function  
684 and regulation of spike architecture. Interestingly, the DNA variation SNP-939 (C/T)  
685 is located in the promoter region of *TaMYB4-A*, right under the WFZP core binding  
686 motif (Figure 8A). This suggested that the C/T SNP may contribute to *TaMYB4-A*  
687 expression difference via affecting WFZP binding. Indeed, we confirmed the WFZP  
688 repressed *TaMYB4-A* via the recognition of the conserved motif, and such repression is  
689 abolished with C-to-T mutation in reporter assay in tobacco leaves (Figure 8B). We  
690 further selected 33 different wheat varieties of the two types (C-type and T-type) to  
691 measure the *TaMYB4-A* expression level and spike morphology. Wheat varieties of C-  
692 type showed elite agronomic traits with longer SL with more FSPS and a significant  
693 higher level of *TaMYB4-A* expression, while the T-type containing wheat varieties  
694 showed shorter SL, less FSPS and lower level of *TaMYB4-A* expression (Figure 8C).  
695 This result provides genetic evidence that the C/T SNP could cause expression level  
696 difference of *TaMYB4-A* and in turn affects SL and FSPS.

697

698 Furthermore, we wonder how this C/T SNP site within *TaMYB4-A* promoter being  
699 selected during the breeding process in China. Based on the exome capture sequencing  
700 data of the Chinese wheat mini-core collection (MCC) (Li et al., 2022a), percentages  
701 of accessions carrying the reference allele (C-type) was considerably higher in  
702 landraces (82.08%) and modern cultivar (78.18%) compared with introduced cultivar  
703 (45.45%) (Figure 8D). Of note, the frequency of C-type was significantly elevated  
704 along with the progress of breeding, indicating that the elite C-type of *TaMYB4-A* has

705 been widely used in the past breeding process of China, especially after year 1978  
706 (Figure 8D). Founder parents have extensively promoted the improvement of wheat  
707 varieties in China since the 1950s, including Zhoumai16, St2422/464, Nanda2419,  
708 Nanda2419, St2422/464, Funo, Xiaoyan6, Aimengniu, Zhou8425B, Abbondanza and  
709 Lovrin10 (Yang et al., 2022). 17 out of 21 founder lines were C-type at SNP-93, except  
710 for Aimengniu (T/T) and Lovrin10 (T/T) (Figure 8E). Importantly, the most widely  
711 grown derived varieties from Aimengniu or Lovrin10 (for instance, Jimai26, Jimai38  
712 and Shi4185 derived from Lovrin10, and Yumai21, Yuejin5, Lumai15, Zhoumai16 and  
713 Zhoumai18 from Aimengniu) are apt to retain the C-type at SNP-939 from another  
714 parent (Figure 8E). Interestingly, the alleles showed distinct distribution characteristics  
715 in the major Chinese agro-ecological zones. The inferior T-type was relatively frequent  
716 ( $\geq 40\%$ ) in spring wheat regions (VI, VII, VIII), followed by winter-spring mixed  
717 regions (IX and X, 22.22% and 23.08% respectively), and appears to be with low  
718 frequency (< 20%) in the winter wheat regions (I, II, III, IV, V). (Figure 8F).  
719  
720 Thus, the elite C-type allele of *TaMYB4-A* is likely originated from Chinese local  
721 germplasm and widely used during the breeding process but still hold the potential to  
722 be used for cultivar improvement for certain wheat production region in China.  
723



724

725 **Figure 8. *TaMYB4-A* has a key SNP at WFZP binding site associate with spike  
726 architecture selection.**

727 (A) Association analysis between genetic variations in *TaMYB4-A*. Dots connected with  
728 the blue dashed lines indicate the variants that are significantly associated with  
729 fertile spikelet number per spike (FSPS). The schematic diagram of the ~6-kb  
730 genomics region of *TaMYB4-A* is shown, followed by a LD plot with white to  
731 black represents  $r^2 = 0-1$ . The SNP-939 was located in the core WFZP DNA-  
732 binding motif. Haplotype of selected 33 varieties for expression level and spike  
733 morphology determination were shown below.

734 (B) Luciferase reporter assays of *TaMYB4-A* promoter activity with the WFZP binding  
735 site C/T. Schematic diagram in the left part showing the vectors used in this array.  
736 Student's *t*-test was used for the statistical significance; \*\*\*,  $P < 0.0001$ ; ns, no  
737 significant difference.

- 738 (C) Spike length and FSPS of cultivars with different haplotypes of *TaMYB4-A* based  
739 on five-point data from two years and their expression level of *TaMYB4-A*. Dots  
740 show data distribution (n=3 or 5 biologically independent samples), *p* values  
741 calculated using two-tailed *t*-test. (D) The percentages of accessions with reference  
742 and alternative allele of SNP-939 in different category (I, left) and breeding  
743 periods (I, right). The line chart shows the allele frequency of reference C-type.  
744 (E) The genotype of wheat founder lines and their derived cultivars. The derived  
745 cultivars of Aimengniu and Lovrin10 were shown in the tree, and cultivars with  
746 reference C-type were in yellow and the T-type in blue.  
747 (F) The percentages of accessions with reference and alternative allele of SNP-939 in  
748 different ecological zones of China. The size of pie charts in the geographical map  
749 showing the number of cultivars, with percentage of the two SNP haplotypes in  
750 different color (C-type, yellow; T-type, blue).  
751

## 752 **Discussion**

753 Wheat is one of the first domesticated crops and domestication is linked with the  
754 modification of inflorescence architecture to ease harvesting and improve grain yield  
755 (Gauley and Boden, 2019). Increasing yields is also one of the primary goals for  
756 breeding. For cereal crops, inflorescence architecture largely determines the grain  
757 productivity via affecting the spikelet and floret development. Better understanding of  
758 the molecular mechanism that governs inflorescence architecture would facilitate the  
759 trait-designed breeding process. As compared to rice, maize and barley (Gao et al.,  
760 2019; Wang et al., 2021; Yuan et al., 2020; Zhang and Yuan, 2014), the genetic and  
761 molecular regulation of spike/inflorescence development in wheat is largely delayed.  
762 Here, we have generated a time-serial epigenomic landscapes consisting of various  
763 types of histone modifications, accessible chromatin, and transcriptomes of wheat shoot  
764 apex from vegetative development to spike architecture formation. This would be a  
765 valuable data resource for systematic study of molecular insights for wheat  
766 inflorescence/spike development and mining of key regulators for shaping spike  
767 architecture (Figure 1).

768

## 769 **Epigenetic layer regulation of vegetative-to-reproductive transition in wheat**

770 The meristem of shoot apex generates different primordium cells for initiation of  
771 various tissues, such as leaf primordia from SAM at vegetative stage, and spikelet

772 primordia from IM during flowering transition. This transition is tightly regulated by  
773 various factors, such as TaTB1, VRN1, TaFT1, Ppd1 via mediating endogenous and  
774 environmental signals (Figure 1D). Here, we found during the transition from SAM to  
775 DR/SMI (vegetative to reproductive growth), the chromatin accessibility is generally  
776 increased (Figure 1G), showing a synchronous pattern with gene activated during floral  
777 induction such as inflorescence meristem identity genes, hormone biosynthesis and  
778 signaling (Figures 2B and 2F). However, open chromatin is not sufficient to active  
779 genes expression, especially when H3K27me3 is covered at the genic region (Figures  
780 2G and 2H). But gain-of chromatin accessibility does set a ‘primed status’ for later  
781 activation of genes when the H3K27me3 is removed at a late developmental stage  
782 (Figures 2G and 2H). Such chromatin status affected genes including well-known  
783 flowering time gene *VRN1*, and genes involved in spikelet meristem formation, such as  
784 *WAP3*, *TaFUL3*. Thus, chromatin layer regulation is associated with the transcriptional  
785 status of key regulators during vegetative-to-reproductive transition in wheat.

786

787 **Integration of TRN with GWAS enables systematic and efficient identification of  
788 key factors in determine inflorescence architecture**

789 The inflorescence of wheat is made up with spikelets and florets harbored within  
790 spikelet. Wheat inflorescence is determined at the time of terminal spikelet formation,  
791 which in turn affects the SNS. Whereas the arrangement of spikelet could influence the  
792 floret development inside. Thus, the initiation, distribution and termination of spikelet  
793 largely shape the inflorescence architecture and grain yield (Gao et al., 2019; Wang et  
794 al., 2021). This is likely driven by identity transition of different primordia cells in the  
795 context of hormone signaling and transcriptional regulatory network (Feng et al., 2017;  
796 Qi et al., 2019). Understanding the main regulatory network and identification of key  
797 factors that driving such network would give us potential candidates for shaping  
798 inflorescence structure. In addition, one could expect that genetic variation on such key  
799 factors within the regulatory network *per se* or variations that changing the regulatory  
800 circuit could generate influence on the outcome of inflorescence architecture.

801

802 Following this logic, by taking advantage of our time-serial profiling of transcriptome  
803 and epigenome dataset, in combination with TF-motif binding information in model  
804 plant (Castro-Mondragon et al., 2022), we build-up a transcriptional regulatory  
805 networks that likely governs the spike formation after floral transition (Figure 3).  
806 Numerous TFs are identified to take part in the TRN, including functional studied  
807 factors such as *VRN1*, *TaTB1*, *TaFUL3* in wheat and TFs from MADS-box, ARF, SPL  
808 families that being reported to regulate inflorescence formation in other crops (Figure  
809 3) (Liu et al., 2022a; Ram et al., 2020; Rong et al., 2018; Wang et al., 2022; Xu et al.,  
810 2016). On top of this, we combined public available GWAS or QTL analysis with focus  
811 on the traits related to spike development to filter for those TFs located within the  
812 GWAS associated genetic regions and have SNP in the regulatory open chromatin  
813 regions that likely affects the transcriptional regulation circuit (Figure 4). This strategy  
814 identified 260 TFs, including 52 functionally analyzed in wheat or other crops. Through  
815 TILLING mutant lines screening, we confirmed mutant lines with 44 novel TFs  
816 showing spike development defects, including initiation, distribution and termination  
817 or degeneration of spikelet or even floret (Figure 6). Thus, such strategy sets a good  
818 example for batch screening factors for agronomic traits in crops.

819

820 **TRN facilitates gene functional study and elite allele discovery in breeding  
821 application**

822 TRN generated not only concentrate the attention for identification of key factors  
823 involved in spike development, but also provide guidance for gene functional study.  
824 This is evidenced by revealing the hierarchy regulation module of known individual  
825 factors such as SPL6-MADS34-MADS15-HMA (Figure 5). Importantly, such  
826 regulation module is relatively conserved within *Triticum* tribe, indicating a broad  
827 application for TRN generated in wheat to be used in other species. What is more, the  
828 regulatory circuit suggested by TRN could promote functional study of novel factor,  
829 for instance *TaMYB4-A* (Figure 7). In addition to the genes regulatory relation, TRN  
830 could enable the identification of critical region with high resolution that mediating  
831 transcriptional regulation. For the case of *TaMYB4-A*, we found the SNP presence in

832 the binding motif of upstream regulator WFZP serves as selection site during the  
833 breeding process in China (Figure 8). The elite allele (C-type) within promoter of  
834 *TaMYB4-A* is likely originated from Chinese local germplasm. The frequency of this  
835 elite allele is sharply increased during the later breeding process might because of the  
836 founder effect.

837  
838 In summary, we integrated multi-omics data to reveal transcriptional regulatory  
839 network and epigenetic dynamic during wheat spike formation. With combination of  
840 GWAS analysis, we have identified dozens of novel factors that shape spike  
841 architecture and revealed that SNP under the WFZP binding site within promoter of  
842 *TaMYB4-A* is critical during the wheat breeding process in China.

843

## 844 **Materials and Methods**

### 845 **Plant materials, growth condition and sampling**

846 The winter wheat cultivar KN9204 was used in this study. The germinated seeds were  
847 treated at 4 °C for 30 days. The seedlings were transplanted into soil and grown in the  
848 greenhouse at 22°C/20°C day/night, under long day conditions (16 h light/8 h dark).  
849 The stage-specific shoot apex of wheat was dissected under the stereomicroscope based  
850 on the anatomic and morphological features, and immediately frozen in liquid nitrogen  
851 and stored at -80°C. About 10 to 50 spikes were pooled for each of biological replicate  
852 for RNA-seq (three replicates), ATAC-seq and CUT&Tag (two replicates) analysis at  
853 eight or five development stages.

854

### 855 **Transgenic wheat plant generation and spike related morphological trait 856 observation**

857 The winter wheat cultivar KN9204 was used to amplify gene sequences and the spring  
858 wheat cultivar Fielder was used to generate transgenic wheat plants. To obtain RNAi  
859 transgenic wheat plants, the specific fragment of *TaSPL6*, *TaMADS34* and *TaMADS15*  
860 was separately amplified and inserted into pc336 (*Ubi:GWRNAi:NOS*) vector using

861 gateway cloning method. All constructed vectors were transformed into callus to  
862 generate the transgenic plants as described previously (Liu et al., 2022b). The pc336  
863 vector was kindly provided by Dr. Daolin Fu at College of Agronomy, Shandong  
864 Agricultural University, Tai'an, Shandong, China.

865

866 The transgenic lines and mutant lines were grown at the Experimental Station of  
867 Institute of Genetics and Developmental Biology, Chinese Academy of Sciences,  
868 Changping, Beijing for 2 consecutive years (planted in September in 2020 and 2021).  
869 Primers for genotyping are listed in Supplemental Table 12.

870

871 The phenotypic traits of mutant lines, T2 generation transgenic and control plants (lines  
872 transformed with an empty vector) which were planted under natural conditions were  
873 recorded for 20 to 40 randomly selected transgenic plants 30 days after flowering.

874

#### 875 **RNA extraction, sequencing, quantitative PCR and *in situ* hybridization**

876 Total RNA was extracted using HiPure Plant RNA Mini Kit according to the  
877 manufacturer's instructions (Magen, R4111-02). RNA-seq libraries construction and  
878 sequencing platform were the same as previous description (Zhao et al., 2022), by  
879 Annoroad Gene Technology.

880

881 First-strand cDNA was synthesized from 2 µg of DNase I-treated total RNA using the  
882 TransScript First Strand cDNA Synthesis SuperMix Kit (TransGen, AT301-02).  
883 Quantitative PCR was performed using the ChamQ Universal SYBR qPCR Master Mix  
884 (Vazyme, Q711-02) by QuantStudio5 (Applied biosystems). Expression of genes of  
885 interest were normalized to Tubulin for calibration, relative expression level is  
886 calculated via the  $2^{\Delta\Delta Ct}$  analysis method (Livak and Schmittgen, 2001). Primers used  
887 for qPCR are listed in Supplemental Table 12.

888

889 RNA *in situ* hybridization was carried out as described previously (Cui et al., 2010).  
890 Fresh young spikes were fixed in formalin-acetic acid-alcohol overnight at 4°C,

891 dehydrated through a standard ethanol series, embedded in Paraplast Plus tissue-  
892 embedding medium (Sigma-Aldrich, P3683), and sectioned at 8  $\mu$ m width using a  
893 microtome (Leica Microsystems, RM2235). Digoxigenin-labeled RNA probes were  
894 synthesized using a DIG northern Starter Kit (Roche, 11277073910), according to the  
895 manufacturer's instructions. Primer sequences used for probe synthesis are listed in  
896 Supplemental Table 12.

897

898 **Data Preprocessing and reads alignment**

899 Raw reads were filtered by fastp v0.20.1 with parameter “--detect\_adapter\_for\_pe” for  
900 adapters removing, low-quality bases trimming, and reads filtering (Chen et al., 2018).  
901 Furthermore, FastQC v0.11.8 ([http://www.bioinformatics.babraham.ac.uk/projects](http://www.bioinformatics.babraham.ac.uk/projects/fastqc/)  
902 /fastqc/) was performed to ensure the high quality of reads.

903

904 Reads were aligned using either BWA-MEM v0.7.17 with parameter “-M” (for ATAC-  
905 seq and CUT&Tag seq) or hisat2 v2.1.0 with default parameters (for RNA-seq) to the  
906 *Triticum aestivum* (Chinese Spring) reference genome (IWGSC RefSeq v1.0,  
907 [https://urgi.versailles.inra.fr/download/iwgsc/IWGSC\\_RefSeq\\_Assemblies/v1.0/](https://urgi.versailles.inra.fr/download/iwgsc/IWGSC_RefSeq_Assemblies/v1.0/))  
908 (Appels et al., 2018; Kim et al., 2019; Li and Durbin, 2009). Gene models from the  
909 IWGSC Annotation v1.1 was used as the reference and high-confidence genes were  
910 used throughout this study. The resulting SAM files were converted to BAM format,  
911 sorted, and indexed using Samtools v1.4 (Danecek et al., 2021). Sam files of RNA-seq  
912 generated from hisat2 were converted to bam files without deduplication. For ATAC-  
913 seq and CUT&Tag, SAM files were further filtered with “samtools view -bS -F 1,804 -  
914 f 2 -q 30” to filter out the low-quality mapped reads. Duplicates in the high-quality  
915 mapped reads were removed using Picard v2.23.3. Two replicates bam files were  
916 merged by samtools. To normalize and visualize the individual and merged replicate  
917 datasets, the BAM files were converted to bigwig files using bamCoverage provided  
918 by deepTools v3.3.0 with 10 bp bin size and normalized by RPKM (Reads Per Kilobase  
919 per Million mapped reads) with parameters “-bs 10 --effectiveGenomeSize  
920 14,600,000,000 --normalizeUsing RPKM --smoothLength 50” (Ramirez et al., 2014).

921

## 922 **RNA-seq data analyses**

923 The number of paired reads that mapping to each gene was counted using feature  
924 Counts v2.0.1 with the parameter "-p" (Liao et al., 2014). The counts files were then  
925 used as inputs for DEGs (differentially expressed genes) analysis by DESeq2 v1.26.0  
926 with a threshold "absolute value of Log2 Fold Change  $\geq 1$  and FDR  $\leq 0.05$ " (Love  
927 et al., 2014). The raw counts were further normalized to TPM (Transcripts Per Kilobase  
928 Million) for gene expression quantification. For subsequent clustering and  
929 visualization, we obtained mean counts by merging three biological replicates. TPM  
930 values of genes were Z-scaled and clustered by k-means method and displayed using R  
931 package ComplexHeatmap (v2.4.3) (Gu et al., 2016). Functional enrichment was  
932 performed using an R package clusterProfiler v3.18.1, and GO annotation files were  
933 generated from IWGSC Annotation v1.1 (Yu et al., 2012).

934

## 935 **Cut&Tag and ATAC-seq experiment and data analyses**

936 ATAC-seq and CUT&Tag experiment were done follow the previous described method  
937 (Zhao et al., 2022). Tn5 transposase used and tagmentation assay is done following the  
938 manual (Vazyme, TD501-01). Libraries were purified with AMPure beads (Beckman,  
939 A63881) and sequenced using the Illumina Novaseq platform at Annoroad Gene  
940 Technology. Antibodies used for histone modifications are listed in Supplemental Table  
941 13.

942

943 Data processing and reads alignment were performed as previously described (Zhao et  
944 al., 2022). MACS2 v2.1.4 was used to call peaks. Parameters "-p 1e-3" was used for  
945 H3K27ac, H3K4me3 and H2A.Z; parameters "--broad --broad-cutoff 0.05" were used  
946 for H3K27me3 and H3K36me3 (Zhang et al., 2008). For ATAC-seq data, MACS2 was  
947 used with parameters "--cutoff-analysis --nomodel --shift -100 --extsize 200". The  
948 peaks were annotated by R package ChIPseeker v1.26.2 with "annotatePeak" function  
949 (Yu et al., 2015). The gene promoters are defined as 3.0 kb upstream of gene TSS.

950

951 For the identification of transcription factor footprints in ATAC-seq peaks, we used the  
952 HINT tool v0.13.2 of the Regulatory Genomics Toolbox (RGT) (Gusmao et al., 2014).  
953 Custom wheat genome was configured using IWGSC refseq v1.1 Chinese Spring  
954 genome based on the introduction of HINT software. TF motifs were downloaded from  
955 JASPAR Plantae database (<https://jaspar.genereg.net/>) (Castro-Mondragon et al.,  
956 2022).

957

### 958 **Differential chromatin modification enriched regions detection**

959 For Cut&Tag and ATAC-seq, reads count and CPM normalized value of peaks were  
960 calculated by R package DiffBind v2.16.2 with the setting  
961 "DBA\_SCORE\_TMM\_READS\_EFFECTIVE\_CPM". DiffBind was also used to  
962 identify differentially accessible regions and histone modification enriched regions with  
963 parameters "method = DBA\_DESEQ2" and a threshold "absolute value of Log2 Fold  
964 Change  $\geq 1$  and FDR  $\leq 0.05$ ".

965

### 966 **Psuedotime indexing and gene regulatory network construction**

967 We used the psuedotime indexing method to analyze gene expression as described in  
968 previous studies with some modifications (Hao et al., 2021; Leiboff and Hake, 2019;  
969 Zhao et al., 2022). All of the expressed genes during spike reproductive development  
970 (From SMI to FOP) were used to separate samples on a PCA plot. Then, each  
971 developmental stage was assigned a location and the Euclidean distance between  
972 adjacent stages was calculated and scaled from 0.0 to 10.0. For each gene, we calculated  
973 the fitted curve and interpolated the curve into 500 points based on gene expression  
974 using the "loess" function in R. We further performed PCA for each gene based on the  
975 standardized expression data and used atan2 function in R to order genes based on the  
976 time of expression.

977

978 For GRNs construction, we only focused on DEGs with TPM values higher than 0.5 in

979 any stages from SMI to FOP. For one gene, its potential upstream regulatory TFs was  
980 predicted based on the motif present at gene regulatory region. Here we firstly used  
981 HINT tool v0.13.2 to identify footprints within ATAC-seq peaks and motifs within the  
982 footprints. Then matched the motifs to TFs based on JASPAR Plantae database. TFs in  
983 wheat were mapped to TFs of JASPAR Plantae database (Castro-Mondragon et al.,  
984 2022) used blastp (v 2.10.1) (Camacho et al., 2009) with criteria “evalue < 1e-10 and  
985 identity > 40%”. In this way, we obtained the regulatory relationship between TFs and  
986 target genes. We further filtered the obtained TF-target regulation according to the  
987 following criteria: Firstly, the TPM values of TFs and target genes must be higher than  
988 0.5 at any stage from SMI to FOP simultaneously. Secondly, we overlapped these TF-  
989 target regulations with WGCNA network constructed based on transcriptome of 8 stage  
990 from SAM to FOP, and only retained TF-target regulations also supported by WGCNA  
991 network. In this way we got the final TF-target gene regulatory network. We used k-  
992 means function in R to cluster genes into 6 categories and performed hypergeometric  
993 test to calculate *P*-value of regulation among gene categories.

994

### 995 **Phylogenetic tree construction**

996 Wheat and maize orthologs were identified by reciprocal BLAST of rice MADS34 and  
997 MADS15 protein sequences. Sequence alignment was performed using MUSCLE  
998 v3.8.1551 (Multiple Protein Sequence Alignment, <http://www.drive5.com/muscle>) with  
999 default settings (Edgar, 2004). We only retained amino acid positions that were present  
1000 in at least 50% of sequences using trimAl v1.4.rev15 (<http://trimal.cgenomics.org>) with  
1001 parameters “-gt 0.5” (Capella-Gutierrez et al., 2009). We used RAxML v8.2.12 to create  
1002 maximum likelihood phylogenetic trees using model PROTGAMMAGTR and 100  
1003 rapid bootstraps (Stamatakis, 2014).

1004

### 1005 **GWAS analysis**

1006 The 319, 558 SNPs (missing rates  $\leq 0.1$ , MAF  $\geq 0.05$ ) from wheat 660K SNP array  
1007 screening of 214 samples were performed to do association analysis with phenotypic  
1008 data, implemented in Tassel v5.2 using the mixed linear model. The threshold for

1009 genome-wide significance was determined by the value 1/independent number of SNPs  
1010 (SNPs of weak LD with other SNPs ( $r^2 < 0.5$ ) were regarded as independent SNPs).  
1011 The genome-wide significant marker-trait associations were identified using a threshold  
1012 cutoff of 3.16E-04. Manhattan plots and quantile-quantile plots were generated using  
1013 R package “CMplot” (<https://github.com/YinLiLin/R-CMplot>).

1014

1015 **Gene based association analysis**

1016 The nucleotide polymorphisms in 6 kb genomic region of *TaMYB4-A*, including exons,  
1017 intron regions, 4 kb promoter regions and 0.5 kb 3'-UTR regions, were identified using  
1018 the whole genome exon capture sequencing data of 287 Chinese wheat mini-core  
1019 collection samples (Li et al., 2022a). Tassel v5.2 was used to establish the association  
1020 of polymorphisms with the FSS, and Haploview 4.2 was used to calculate the pairwise  
1021 linkage disequilibrium and draw the LD plot.

1022

1023 **Spike morphology observation by scanning electron microscopy (SEM)**

1024 Photomicrographs of young spikes were taken using a stereomicroscope (S8 APO,  
1025 Leica Microsystems) equipped with a digital camera (Canon, A640). For SEM, young  
1026 spikes from each stage were fixed in 2.5% glutaraldehyde at 4°C. After dehydration in  
1027 a series of ethanol solutions and substitution with 3-methylbutyl acetate, the samples  
1028 were subjected to critical point drying, coated with platinum, and observed using a  
1029 variable pressure scanning electron microscope (Hitachi S-3000N).

1030

1031 **Luciferase (LUC) reporter assay**

1032 For LUC analyses, full-length coding sequences of *TaSPL6*, *TaMADS34*, and  
1033 *TaMADS15*, *TaMYB4-A*, *WFZP*, *TaDOF17* were cloned into PTF101 vector to generate  
1034 the effector construct *35Spro: TF-GFP*, and about 3 Kb promoter fragment of  
1035 *TaMADS34*, *TaMADS15*, *TaHMA*, *TaMYB4-A*, *TaAP2-39*, *TaI-BAK1* and *TaPILS7*  
1036 were amplified and fused in-frame with the CP461-LUC vector to generate the reporter  
1037 construct *target-pro: LUC* (see Supplemental Table 12 for primers). The plasmids were  
1038 transformed into Agrobacterium GV3101. The mixture of bacterial solution

1039 35S<sub>pro</sub>:TF-GFP (OD=0.5), target-pro:LUC (OD=0.5) and P19 (OD=0.3) in activation  
1040 buffer (10 mM MES, 150 μM AS, 10 mM MgCl<sub>2</sub>) was injected to tobacco (*Nicotiana*  
1041 *benthamiana*). pSUPER-GFP, target-pro:LUC and P19 as control. Firefly luciferase  
1042 (LUC) and Renilla luciferase (REN) activities were measured using dual luciferase  
1043 assay reagent (Promega, VPE1910) after 1 day' co-cultivation in dark and 2 days in  
1044 light, the relative value of LUC/REN is indicated as average with standard error of  
1045 multiple replicates.

1046

#### 1047 **Statistics and data visualization**

1048 R (<https://cran.r-project.org/>; version 4.0.2) was used to compute statistics and generate  
1049 plots if not specified. For two groups' comparison of data, the student's t-test was used,  
1050 such as Figure 3H, 5D, 5E, 7F, 7G, 8B, 8C, and Supplemental Figure 5A. For  
1051 enrichment analysis, Fisher's exact test was used, such as Figure 2C, 2E, Figure3B, 3C,  
1052 4H, and Supplemental Figure 2C, 2D. For three or more independent groups  
1053 comparison of data, Fisher's Least Significant Difference (LSD) was used, such as  
1054 Figure 5D, 6D, 7E, and Supplemental Figure 5B, 6A, 6C, 6D, 7B, 7C.

1055

#### 1056 **Data availability**

1057 The raw sequence data reported in this paper have been deposited in the Genome  
1058 Sequence Archive (Chen et al., 2021) in National Genomics Data Center (CNCB-  
1059 NGDC Members and Partners, 2022), China National Center for Bioinformation /  
1060 Beijing Institute of Genomics, Chinese Academy of Sciences (PRJCA013096) that are  
1061 publicly accessible at <https://ngdc.cncb.ac.cn/gsa>

1062

#### 1063 **Acknowledgements**

1064 We thank X.G. Liu (College of Life Sciences, Hebei Normal University) for the wheat  
1065 WFZP-OE seeds. This research is supported by the National Natural Sciences  
1066 Foundation of China (31921005), Strategic Priority Research Program of the Chinese  
1067 Academy of Sciences (XDA24010204), National Key Research and Development

1068 Program of China (2021YFD1201500), and the Major Basic Research Program of  
1069 Shandong Natural Science Foundation (ZR2019ZD15).

1070

## 1071 **Author contributions**

1072 J.X. designed and supervised the research, J.X., X.-L. L., Y.-X.X., D.-Z.W. wrote the  
1073 manuscript. X.-L. L. did the sample collection and *in situ* hybridization; X.-L. L. and  
1074 X.-Y.Z. did plasmid construction and qRT-PCR. X.-M.B. did wheat transformation;  
1075 X.-L. L. and Y.-M.Y. performed CUT&Tag, ATAC-seq and RNA-seq experiments;  
1076 X.-Y. Z. and H.-Z. W. did the reporter assay; Y.-L.D., X.-Y.Z., F.L., X.-S.Z. and X.-  
1077 D.F. provide some raw data or plant materials; X.-Y. X., D.-Z. W. performed bio-  
1078 informatics analysis; J.-F. J., X.-Y.Z., F.L., X.-S. Z. and X.-D.F. polished the  
1079 manuscript; X.-L. L., Y.-X. X., D.-Z.W., Y.-M.Y. and J.X. prepared all the figures. All  
1080 authors discussed the results and commented on the manuscript.

1081

## 1082 **Competing interests**

1083 The authors declare no competing interests

1084

## 1085 **References**

1086

- 1087 **Appels, R., Eversole, K., Feuillet, C., Keller, B., Rogers, J., Stein, N., Pozniak, C.J.,**  
1088 **Choulet, F., Distelfeld, A., Poland, J., et al. (2018). Shifting the limits in wheat research and**  
1089 **breeding using a fully annotated reference genome. Science 361:661. eaar7191**  
1090 **10.1126/science.aar7191.**
- 1091 **Boden, S.A., Cavanagh, C., Cullis, B.R., Ramm, K., Greenwood, J., Finnegan, E.J.,**  
1092 **Trevaskis, B., and Swain, S.M. (2015). Ppd-1 is a key regulator of inflorescence architecture**  
1093 **and paired spikelet development in wheat. Nature Plants 1:1-6. 10.1038/Nplants.2014.16.**
- 1094 **Bonnett, O.T. (1936). The development of the wheat spike. J Agric Res 53:0445-0451.**
- 1095 **Buenrostro, J.D., Wu, B., Chang, H.Y., and Greenleaf, W.J. (2015). ATAC-seq: A Method**  
1096 **for Assaying Chromatin Accessibility Genome-Wide. Curr Protoc Mol Biol 109:21.29.21-**  
1097 **21.29.29. 10.1002/0471142727.mb2129s109.**
- 1098 **Camacho, C., Coulouris, G., Avagyan, V., Ma, N., Papadopoulos, J., Bealer, K., and**  
1099 **Madden, T.L. (2009). BLAST+: architecture and applications. BMC Bioinformatics 10:421.**  
1100 **10.1186/1471-2105-10-421.**

- 1101 **Cao, J., Liu, K., Song, W., Zhang, J., Yao, Y., Xin, M., Hu, Z., Peng, H., Ni, Z., Sun, Q., et**  
1102 **al. (2021). Pleiotropic function of the SQUAMOSA PROMOTER-BINDING PROTEIN-LIKE**  
1103 **gene TaSPL14 in wheat plant architecture. *Planta* **253**:44. 10.1007/s00425-020-03531-x.**
- 1104 **Capella-Gutierrez, S., Silla-Martinez, J.M., and Gabaldon, T. (2009). trimAl: a tool for**  
1105 **automated alignment trimming in large-scale phylogenetic analyses. *Bioinformatics* **25**:1972-**  
1106 **1973. 10.1093/bioinformatics/btp348.**
- 1107 **Castro-Mondragon, J.A., Riudavets-Puig, R., Rauluseviciute, I., Lemma, R.B., Turchi, L.,**  
1108 **Blanc-Mathieu, R., Lucas, J., Boddie, P., Khan, A., Manosalva Perez, N., et al. (2022).**  
1109 **JASPAR 2022: the 9th release of the open-access database of transcription factor binding**  
1110 **profiles. *Nucleic Acids Res* **50**:D165-D173. 10.1093/nar/gkab1113.**
- 1111 **Chen, S., Zhou, Y., Chen, Y., and Gu, J. (2018). fastp: an ultra-fast all-in-one FASTQ**  
1112 **preprocessor. *Bioinformatics* **34**:i884-i890. 10.1093/bioinformatics/bty560.**
- 1113 **Chen, T., Chen, X., Zhang, S., Zhu, J., Tang, B., Wang, A., Dong, L., Zhang, Z., Yu, C.,**  
1114 **Sun, Y., et al. (2021). The Genome Sequence Archive Family: Toward Explosive Data Growth**  
1115 **and Diverse Data Types. *Genomics Proteomics Bioinformatics* **19**:578-583.**  
1116 **10.1016/j.gpb.2021.08.001.**
- 1117 **Cui, R., Han, J., Zhao, S., Su, K., Wu, F., Du, X., Xu, Q., Chong, K., Theissen, G., and**  
1118 **Meng, Z. (2010). Functional conservation and diversification of class E floral homeotic genes**  
1119 **in rice (*Oryza sativa*). *Plant J* **61**:767-781. 10.1111/j.1365-313X.2009.04101.x.**
- 1120 **Danecek, P., Bonfield, J.K., Liddle, J., Marshall, J., Ohan, V., Pollard, M.O., Whitwham,**  
1121 **A., Keane, T., McCarthy, S.A., Davies, R.M., et al. (2021). Twelve years of SAMtools and**  
1122 **BCFtools. *Gigascience* **10**10.1093/gigascience/giab008.**
- 1123 **Debernardi, J.M., Greenwood, J.R., Jean Finnegan, E., Jernstedt, J., and Dubcovsky, J.**  
1124 **(2020). APETALA 2-like genes AP2L2 and Q specify lemma identity and axillary floral**  
1125 **meristem development in wheat. *Plant J* **101**:171-187. 10.1111/tpj.14528.**
- 1126 **Dixon, L.E., Greenwood, J.R., Bencivenga, S., Zhang, P., Cockram, J., Mellers, G., Ramm,**  
1127 **K., Cavanagh, C., Swain, S.M., and Boden, S.A. (2018). TEOSINTE BRANCHED1**  
1128 **Regulates Inflorescence Architecture and Development in Bread Wheat (*Triticum aestivum*). *Plant Cell* **30**:563-581. 10.1105/tpc.17.00961.**
- 1129 **Dobrovolskaya, O., Pont, C., Sibout, R., Martinek, P., Badaeva, E., Murat, F., Chosson,**  
1130 **A., Watanabe, N., Prat, E., Gautier, N., et al. (2015). FRIZZY PANICLE drives**  
1131 **supernumerary spikelets in bread wheat. *Plant Physiol* **167**:189-199. 10.1104/pp.114.250043.**
- 1132 **Doebley, J., Stec, A., and Hubbard, L. (1997). The evolution of apical dominance in maize. *Nature* **386**:485-488. 10.1038/386485a0.**
- 1133 **Du, D., Zhang, D., Yuan, J., Feng, M., Li, Z., Wang, Z., Zhang, Z., Li, X., Ke, W., Li, R.,**  
1134 **et al. (2021). FRIZZY PANICLE defines a regulatory hub for simultaneously controlling**  
1135 **spikelet formation and awn elongation in bread wheat. *New Phytol* **231**:814-833.**  
1136 **10.1111/nph.17388.**
- 1137 **Edgar, R.C. (2004). MUSCLE: a multiple sequence alignment method with reduced time and**  
1138 **space complexity. *BMC Bioinformatics* **5**:113. 10.1186/1471-2105-5-113.**
- 1139 **Feng, N., Song, G.Y., Guan, J.T., Chen, K., Jia, M.L., Huang, D.H., Wu, J.J., Zhang, L.C.,**  
1140 **Kong, X.Y., Geng, S.F., et al. (2017). Transcriptome Profiling of Wheat Inflorescence**  
1141 **Development from Spikelet Initiation to Floral Patterning Identified Stage-Specific Regulatory**  
1142 **Genes. *Plant Physiol* **174**:1779-1794. 10.1104/pp.17.00310.**

- 1145 **Finnegan, E.J., Ford, B., Wallace, X., Pettolino, F., Griffin, P.T., Schmitz, R.J., Zhang, P.,**  
1146 **Barrero, J.M., Hayden, M.J., Boden, S.A., et al.** (2018). Zebularine treatment is associated  
1147 with deletion of FT-B1 leading to an increase in spikelet number in bread wheat. *Plant Cell*  
1148 *Environ* **41**:1346-1360. 10.1111/pce.13164.
- 1149 **Gao, X.Q., Wang, N., Wang, X.L., and Zhang, X.S.** (2019). Architecture of Wheat  
1150 Inflorescence: Insights from Rice. *Trends Plant Sci* 10.1016/j.tplants.2019.06.002.
- 1151 **Gauley, A., and Boden, S.A.** (2019). Genetic pathways controlling inflorescence architecture  
1152 and development in wheat and barley. *J Integr Plant Biol* **61**:296-309. 10.1111/jipb.12732.
- 1153 **Gu, Z., Eils, R., and Schlesner, M.** (2016). Complex heatmaps reveal patterns and correlations  
1154 in multidimensional genomic data. *Bioinformatics* **32**:2847-2849.  
1155 10.1093/bioinformatics/btw313.
- 1156 **Guo, L.J., Ma, M., Wu, L.N., Zhou, M.D., Li, M.Y., Wu, B.W., Li, L., Liu, X.L., Jing, R.L.,**  
1157 **Chen, W., et al.** (2022). Modified expression of TaCYP78A5 enhances grain weight with yield  
1158 potential by accumulating auxin in wheat (*Triticum aestivum* L.). *Plant Biotechnology Journal*  
1159 **20**:168-182. 10.1111/pbi.13704.
- 1160 **Gusmao, E.G., Dieterich, C., Zenke, M., and Costa, I.G.** (2014). Detection of active  
1161 transcription factor binding sites with the combination of DNase hypersensitivity and histone  
1162 modifications. *Bioinformatics* **30**:3143-3151. 10.1093/bioinformatics/btu519.
- 1163 **Hao, C.Y., Jiao, C.Z., Hou, J., Li, T., Liu, H.X., Wang, Y.Q., Zheng, J., Liu, H., Bi, Z.H.,**  
1164 **Xu, F.F., et al.** (2020). Resequencing of 145 Landmark Cultivars Reveals Asymmetric Sub-  
1165 genome Selection and Strong Founder Genotype Effects on Wheat Breeding in China. *Mol*  
1166 *Plant* **13**:1733-1751. 10.1016/j.molp.2020.09.001.
- 1167 **Hao, Z., Zhang, Z., Xiang, D., Venglat, P., Chen, J., Gao, P., Datla, R., and Weijers, D.**  
1168 (2021). Conserved, divergent and heterochronic gene expression during Brachypodium and  
1169 Arabidopsis embryo development. *Plant Reprod* **34**:207-224. 10.1007/s00497-021-00413-4.
- 1170 **Jablonski, B., Ogonowska, H., Szala, K., Bajguz, A., Orczyk, W., and Nadolska-Orczyk,**  
1171 **A.** (2020). Silencing of TaCKX1 Mediates Expression of Other TaCKX Genes to Increase Yield  
1172 Parameters in Wheat. *Int J Mol Sci* **21**:10.3390/ijms21134809.
- 1173 **Jablonski, B., Szala, K., Przyborowski, M., Bajguz, A., Chmur, M., Gasparis, S., Orczyk,**  
1174 **W., and Nadolska-Orczyk, A.** (2021). TaCKX2.2 Genes Coordinate Expression of Other  
1175 TaCKX Family Members, Regulate Phytohormone Content and Yield-Related Traits of Wheat.  
1176 *Int J Mol Sci* **22**:10.3390/ijms22084142.
- 1177 **Kaya-Okur, H.S., Wu, S.J., Codomo, C.A., Pledger, E.S., Bryson, T.D., Henikoff, J.G.,**  
1178 **Ahmad, K., and Henikoff, S.** (2019). CUT&Tag for efficient epigenomic profiling of small  
1179 samples and single cells. *Nat Commun* **10**:1930. 10.1038/s41467-019-09982-5.
- 1180 **Kellogg, E.A.** (2022). Genetic control of branching patterns in grass inflorescences. *Plant Cell*  
1181 **34**:2518-2533. 10.1093/plcell/koac080.
- 1182 **Khew, C.Y., Teo, C.J., Chan, W.S., Wong, H.L., Namasivayam, P., and Ho, C.L.** (2015).  
1183 Brassinosteroid insensitive 1-associated kinase 1 (OsI-BAK1) is associated with grain filling  
1184 and leaf development in rice. *J Plant Physiol* **182**:23-32. 10.1016/j.jplph.2015.05.003.
- 1185 **Kim, D., Paggi, J.M., Park, C., Bennett, C., and Salzberg, S.L.** (2019). Graph-based genome  
1186 alignment and genotyping with HISAT2 and HISAT-genotype. *Nat Biotechnol* **37**:907-915.  
1187 10.1038/s41587-019-0201-4.
- 1188 **Klemm, S.L., Shipony, Z., and Greenleaf, W.J.** (2019). Chromatin accessibility and the

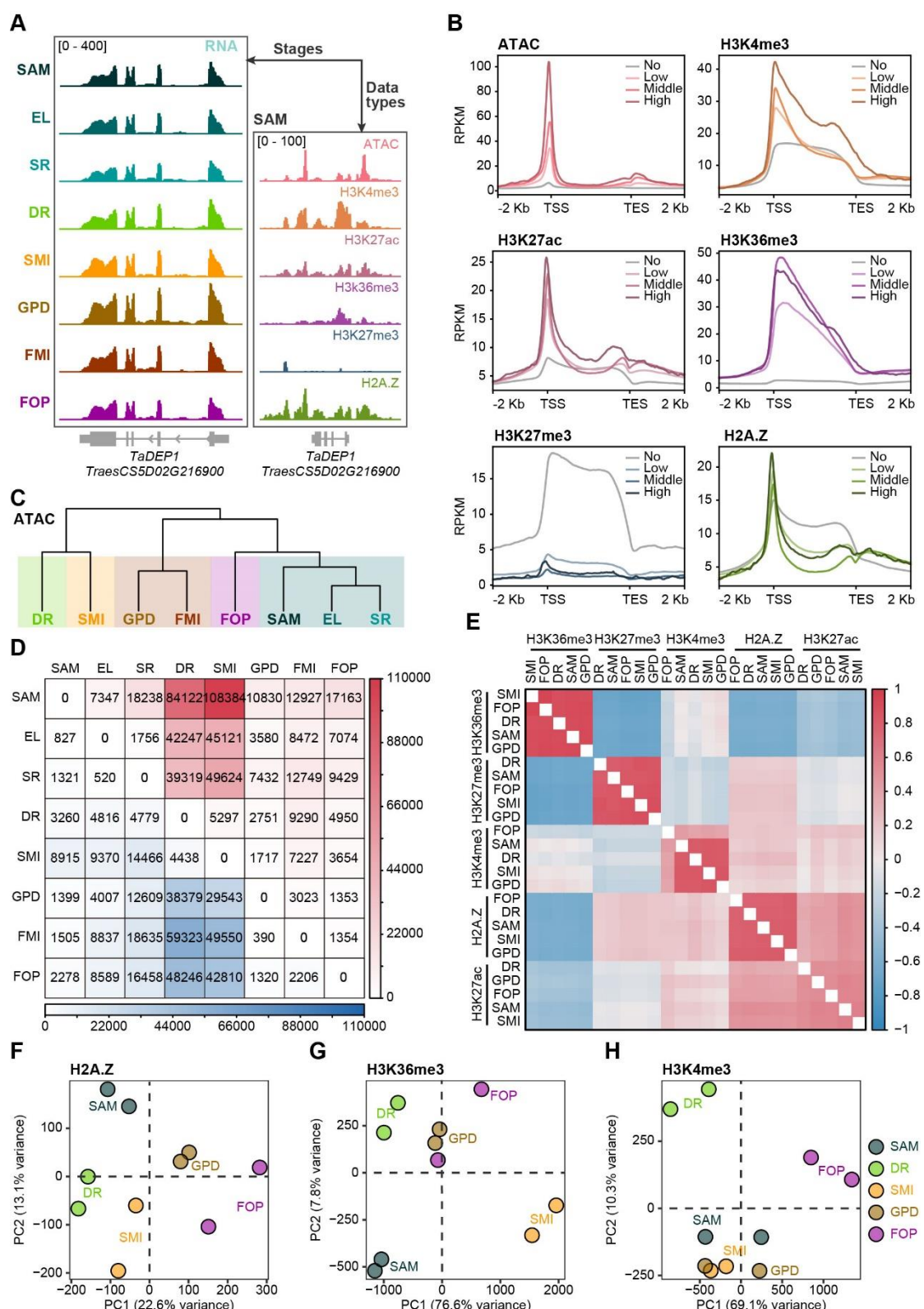
- 1189 regulatory epigenome. *Nat Rev Genet* **20**:207-220. 10.1038/s41576-018-0089-8.
- 1190 **Kobayashi, K., Maekawa, M., Miyao, A., Hirochika, H., and Kyozuka, J.** (2010). PANICLE
- 1191 PHYTOMER2 (PAP2), encoding a SEPALLATA subfamily MADS-box protein, positively
- 1192 controls spikelet meristem identity in rice. *Plant and Cell Physiology* **51**:47-57.
- 1193 10.1093/pcp/pcp166.
- 1194 **Kobayashi, K., Yasuno, N., Sato, Y., Yoda, M., Yamazaki, R., Kimizu, M., Yoshida, H.,**
- 1195 **Nagamura, Y., and Kyozuka, J.** (2012). Inflorescence Meristem Identity in Rice Is Specified
- 1196 by Overlapping Functions of Three AP1/FUL-Like MADS Box Genes and PAP2, a
- 1197 SEPALLATA MADS Box Gene. *Plant Cell* **24**:1848-1859. 10.1105/tpc.112.097105.
- 1198 **Kong, X.C., Wang, F., Geng, S.F., Guan, J.T., Tao, S., Jia, M.L., Sun, G.L., Wang, Z.Y.,**
- 1199 **Wang, K., Ye, X.G., et al.** (2022). The wheat AGL6-like MADS-box gene is a master regulator
- 1200 for floral organ identity and a target for spikelet meristem development manipulation. *Plant*
- 1201 *Biotechnology Journal* **20**:75-88. 10.1111/pbi.13696.
- 1202 **Koppolu, R., Chen, S., and Schnurbusch, T.** (2022). Evolution of inflorescence branch
- 1203 modifications in cereal crops. *Curr Opin Plant Biol* **65**:102168. 10.1016/j.pbi.2021.102168.
- 1204 **Krasileva, K.V., Vasquez-Gross, H.A., Howell, T., Bailey, P., Paraiso, F., Clissold, L.,**
- 1205 **Simmonds, J., Ramirez-Gonzalez, R.H., Wang, X.D., Borrill, P., et al.** (2017). Uncovering
- 1206 hidden variation in polyploid wheat. *P Natl Acad Sci USA* **114**:E913-E921.
- 1207 10.1073/pnas.1619268114.
- 1208 **Kuzay, S., Lin, H., Li, C., Chen, S., Woods, D.P., Zhang, J., Lan, T., von Korff, M., and**
- 1209 **Dubcovsky, J.** (2022). WAPO-A1 is the causal gene of the 7AL QTL for spikelet number per
- 1210 spike in wheat. *PLoS Genet* **18**:e1009747. 10.1371/journal.pgen.1009747.
- 1211 **Kuzay, S., Xu, Y., Zhang, J., Katz, A., Pearce, S., Su, Z., Fraser, M., Anderson, J.A.,**
- 1212 **Brown-Guedira, G., DeWitt, N., et al.** (2019). Identification of a candidate gene for a QTL
- 1213 for spikelet number per spike on wheat chromosome arm 7AL by high-resolution genetic
- 1214 mapping. *Theor Appl Genet* **132**:2689-2705. 10.1007/s00122-019-03382-5.
- 1215 **Lee, Z.H., Hirakawa, T., Yamaguchi, N., and Ito, T.** (2019). The Roles of Plant Hormones
- 1216 and Their Interactions with Regulatory Genes in Determining Meristem Activity. *International*
- 1217 *Journal of Molecular Sciences* **20ARTN 4065** 10.3390/ijms20164065.
- 1218 **Leiboff, S., and Hake, S.** (2019). Reconstructing the Transcriptional Ontogeny of Maize and
- 1219 Sorghum Supports an Inverse Hourglass Model of Inflorescence Development. *Curr Biol*
- 1220 **29**:3410-3419 e3413. 10.1016/j.cub.2019.08.044.
- 1221 **Li, A., Hao, C., Wang, Z., Geng, S., Jia, M., Wang, F., Han, X., Kong, X., Yin, L., Tao, S.,**
- 1222 **et al.** (2022a). Wheat breeding history reveals synergistic selection of pleiotropic genomic sites
- 1223 for plant architecture and grain yield. *Mol Plant* **15**:504-519. 10.1016/j.molp.2022.01.004.
- 1224 **Li, C., Lin, H., Chen, A., Lau, M., Jernstedt, J., and Dubcovsky, J.** (2019). Wheat VRN1,
- 1225 FUL2 and FUL3 play critical and redundant roles in spikelet development and spike
- 1226 determinacy. *Development* **146**10.1242/dev.175398.
- 1227 **Li, H., and Durbin, R.** (2009). Fast and accurate short read alignment with Burrows-Wheeler
- 1228 transform. *Bioinformatics* **25**:1754-1760. 10.1093/bioinformatics/btp324.
- 1229 **Li, L., Shi, F., Wang, G.L., Guan, Y.B., Zhang, Y.F., Chen, M.J., Chang, J.L., Yang, G.X.,**
- 1230 **He, G.Y., Wang, Y.S., et al.** (2022b). Conservation and Divergence of SQUAMOSA-
- 1231 PROMOTER BINDING PROTEIN-LIKE (SPL) Gene Family between Wheat and Rice.
- 1232 *International Journal of Molecular Sciences* **23ARTN 2099** 10.3390/ijms23042099.

- 1233 **Li, L., Shi, F., Wang, Y., Yu, X., Zhi, J., Guan, Y., Zhao, H., Chang, J., Chen, M., Yang, G.,**  
1234 **et al.** (2020). TaSPL13 regulates inflorescence architecture and development in transgenic  
1235 wheat (*Triticum aestivum* L.). *Plant Sci* **296**:110516. 10.1016/j.plantsci.2020.110516.
- 1236 **Li, Y., Fu, X., Zhao, M., Zhang, W., Li, B., An, D., Li, J., Zhang, A., Liu, R., and Liu, X.**  
1237 (2018). A Genome-wide View of Transcriptome Dynamics During Early Spike Development  
1238 in Bread Wheat. *Sci Rep* **8**:15338. 10.1038/s41598-018-33718-y.
- 1239 **Li, Y., Li, L., Zhao, M., Guo, L., Guo, X., Zhao, D., Batool, A., Dong, B., Xu, H., Cui, S.,**  
1240 **et al.** (2021). Wheat FRIZZY PANICLE activates VERNALIZATION1-A and HOMEOBOX4-  
1241 A to regulate spike development in wheat. *Plant Biotechnol J* 10.1111/pbi.13535.
- 1242 **Liao, Y., Smyth, G.K., and Shi, W.** (2014). featureCounts: an efficient general purpose  
1243 program for assigning sequence reads to genomic features. *Bioinformatics* **30**:923-930.  
1244 10.1093/bioinformatics/btt656.
- 1245 **Lin, X.L., Wu, F., Du, X.Q., Shi, X.W., Liu, Y., Liu, S.J., Hu, Y.X., Theissen, G., and Meng,**  
1246 **Z.** (2014). The pleiotropic SEPALLATA- like gene OsMADS34 reveals that the 'empty glumes'  
1247 of rice (*Oryza sativa*) spikelets are in fact rudimentary lemmas. *New Phytologist* **202**:689-702.  
1248 10.1111/nph.12657.
- 1249 **Liu, J., Shi, X., Chang, Z., Ding, Y., and Ding, C.** (2022a). Auxin Efflux Transporters  
1250 OsPIN1c and OsPIN1d Function Redundantly in Regulating Rice (*Oryza sativa* L.) Panicle  
1251 Development. *Plant Cell Physiol* **63**:305-316. 10.1093/pcp/pcab172.
- 1252 **Liu, X., Bie, X., Lin, X., Li, M., Wang, H., Zhang, X., Yang, Y., Zhang, C., Zhang, X., and**  
1253 **Xiao, J.** (2022b). Uncovering transcriptional regulatory network during regeneration for  
1254 boosting wheat transformation. *bioRxiv* <https://doi.org/10.1101/2022.10.21.513305>.
- 1255 **Livak, K.J., and Schmittgen, T.D.** (2001). Analysis of relative gene expression data using  
1256 real-time quantitative PCR and the 2(T)(-Delta Delta C) method. *Methods* **25**:402-408.  
1257 10.1006/meth.2001.1262.
- 1258 **Love, M.I., Huber, W., and Anders, S.** (2014). Moderated estimation of fold change and  
1259 dispersion for RNA-seq data with DESeq2. *Genome Biol* **15**:550. 10.1186/s13059-014-0550-  
1260 8.
- 1261 **Meng, Q., Li, X., Zhu, W., Yang, L., Liang, W., Dreni, L., and Zhang, D.** (2017). Regulatory  
1262 network and genetic interactions established by OsMADS34 in rice inflorescence and spikelet  
1263 morphogenesis. *J Integr Plant Biol* **59**:693-707. 10.1111/jipb.12594.
- 1264 **Pang, Y., Liu, C., Wang, D., St Amand, P., Bernardo, A., Li, W., He, F., Li, L., Wang, L.,**  
1265 **Yuan, X., et al.** (2020). High-Resolution Genome-wide Association Study Identifies Genomic  
1266 Regions and Candidate Genes for Important Agronomic Traits in Wheat. *Mol Plant* **13**:1311-  
1267 1327. 10.1016/j.molp.2020.07.008.
- 1268 **Perez-Gianmarco, T.I., Severini, A.D., and Gonzalez, F.G.** (2020). Photoperiod-sensitivity  
1269 genes (Ppd-1): quantifying their effect on the photoperiod response model in wheat. *Journal of*  
1270 *Experimental Botany* **71**:1185-1198. 10.1093/jxb/erz483.
- 1271 **Qi, P.F., Jiang, Y.F., Guo, Z.R., Chen, Q., Ouellet, T., Zong, L.J., Wei, Z.Z., Wang, Y.,**  
1272 **Zhang, Y.Z., Xu, B.J., et al.** (2019). Transcriptional reference map of hormone responses in  
1273 wheat spikes. *BMC Genomics* **20**:390. 10.1186/s12864-019-5726-x.
- 1274 **Ram, H., Sahadevan, S., Gale, N., Caggiano, M.P., Yu, X.L., Ohno, C., and Heisler, M.G.**  
1275 (2020). An integrated analysis of cell-type specific gene expression reveals genes regulated by  
1276 REVOLUTA and KANADI1 in the *Arabidopsis* shoot apical meristem. *Plos Genetics* **16**ARTN

- 1277 e1008661 10.1371/journal.pgen.1008661.
- 1278 **Ramirez, F., Dundar, F., Diehl, S., Gruning, B.A., and Manke, T.** (2014). deepTools: a  
1279 flexible platform for exploring deep-sequencing data. *Nucleic Acids Res* **42**:W187-191.  
1280 10.1093/nar/gku365.
- 1281 **Rong, X.F., Sang, Y.L., Wang, L., Meng, W.J., Zou, C.H., Dong, Y.X., Bie, X.M., Cheng,  
1282 Z.J., and Zhang, X.S.** (2018). Type-B ARR<sub>s</sub> Control Carpel Regeneration Through Mediating  
1283 AGAMOUS Expression in *Arabidopsis*. *Plant and Cell Physiology* **59**:761-769.  
1284 10.1093/pcp/pcx187.
- 1285 **Sakuma, S., Golan, G., Guo, Z., Ogawa, T., Tagiri, A., Sugimoto, K., Bernhardt, N.,  
1286 Brassac, J., Mascher, M., Hensel, G., et al.** (2019). Unleashing floret fertility in wheat through  
1287 the mutation of a homeobox gene. *Proc Natl Acad Sci U S A* **116**:5182-5187.  
1288 10.1073/pnas.1815465116.
- 1289 **Sehgal, D., and Dreisigacker, S.** (2022). GWAS Case Studies in Wheat. *Methods Mol Biol*  
1290 **2481**:341-351. 10.1007/978-1-0716-2237-7\_19.
- 1291 **Stamatakis, A.** (2014). RAxML version 8: a tool for phylogenetic analysis and post-analysis  
1292 of large phylogenies. *Bioinformatics* **30**:1312-1313. 10.1093/bioinformatics/btu033.
- 1293 **Sun, C.W., Zhang, F.Y., Yan, X.F., Zhang, X.F., Dong, Z.D., Cui, D.Q., and Chen, F.** (2017).  
1294 Genome-wide association study for 13 agronomic traits reveals distribution of superior alleles  
1295 in bread wheat from the Yellow and Huai Valley of China. *Plant Biotechnology Journal* **15**:953-  
1296 969. 10.1111/pbi.12690.
- 1297 **Uauy, C., Paraiso, F., Colasuonno, P., Tran, R.K., Tsai, H., Berardi, S., Comai, L., and  
1298 Dubcovsky, J.** (2009). A modified TILLING approach to detect induced mutations in tetraploid  
1299 and hexaploid wheat. *BMC Plant Biol* **9**:115. 10.1186/1471-2229-9-115.
- 1300 **VanGessel, C., Hamilton, J., Tabbita, F., Dubcovsky, J., and Pearce, S.** (2022).  
1301 Transcriptional signatures of wheat inflorescence development. *Sci Rep* **12**:17224.  
1302 10.1038/s41598-022-21571-z.
- 1303 **Wang, C., Yang, X., and Li, G.** (2021). Molecular Insights into Inflorescence Meristem  
1304 Specification for Yield Potential in Cereal Crops. *Int J Mol Sci* **22**:10.3390/ijms22073508.
- 1305 **Wang, K., Tang, D., Hong, L., Xu, W., Huang, J., Li, M., Gu, M., Xue, Y., and Cheng, Z.**  
1306 (2010). DEP and AFO regulate reproductive habit in rice. *PLoS Genet* **6**:e1000818.  
1307 10.1371/journal.pgen.1000818.
- 1308 **Wang, Q.L., Sun, A.Z., Chen, S.T., Chen, L.S., and Guo, F.Q.** (2018). SPL6 represses  
1309 signalling outputs of ER stress in control of panicle cell death in rice. *Nat Plants* **4**:280-288.  
1310 10.1038/s41477-018-0131-z.
- 1311 **Wang, Y., Yu, H., Tian, C., Sajjad, M., Gao, C., Tong, Y., Wang, X., and Jiao, Y.** (2017).  
1312 Transcriptome Association Identifies Regulators of Wheat Spike Architecture. *Plant Physiol*  
1313 **175**:746-757. 10.1104/pp.17.00694.
- 1314 **Wang, Y., Du, F., Wang, J., Wang, K., Tian, C., Qi, X., Lu, F., Liu, X., Ye, X., and Jiao, Y.**  
1315 (2022). Improving bread wheat yield through modulating an unselected AP2/ERF gene. *Nat  
1316 Plants* 10.1038/s41477-022-01197-9.
- 1317 **Wu, F., Shi, X., Lin, X., Liu, Y., Chong, K., Theissen, G., and Meng, Z.** (2017). The ABCs  
1318 of flower development: mutational analysis of AP1/FUL-like genes in rice provides evidence  
1319 for a homeotic (A)-function in grasses. *Plant J* **89**:310-324. 10.1111/tpj.13386.
- 1320 **Xiao, J., Liu, B., Yao, Y.Y., Guo, Z.F., Jia, H.Y., Kong, L.R., Zhang, A.M., Ma, W.J., Ni,**

- 1321 **Z.F., Xu, S.B., et al.** (2022). Wheat genomic study for genetic improvement of traits in China.  
1322 *Science China-Life Sciences* **65**:1718-1775. 10.1007/s11427-022-2178-7.
- 1323 **Xu, M., Hu, T., Zhao, J., Park, M.Y., Earley, K.W., Wu, G., Yang, L., and Poethig, R.S.**  
1324 (2016). Developmental Functions of miR156-Regulated SQUAMOSA PROMOTER  
1325 BINDING PROTEIN-LIKE (SPL) Genes in *Arabidopsis thaliana*. *PLoS Genet* **12**:e1006263.  
1326 10.1371/journal.pgen.1006263.
- 1327 **Yaish, M.W., El-kereamy, A., Zhu, T., Beatty, P.H., Good, A.G., Bi, Y.M., and Rothstein, S.J.** (2010). The APETALA-2-Like Transcription Factor OsAP2-39 Controls Key Interactions  
1328 between Abscisic Acid and Gibberellin in Rice. *Plos Genetics* **6**ARTN e1001098  
1329 10.1371/journal.pgen.1001098.
- 1330 **Yang, Z., Wang, Z., Wang, W., Xie, X., Chai, L., Wang, X., Feng, X., Li, J., Peng, H., Su, Z., et al.** (2022). ggComp enables dissection of germplasm resources and construction of a  
1331 multiscale germplasm network in wheat. *Plant Physiol* **188**:1950-1965.  
1332 10.1093/plphys/kiac029.
- 1333 **Yu, G., Wang, L.G., and He, Q.Y.** (2015). ChIPseeker: an R/Bioconductor package for ChIP  
1334 peak annotation, comparison and visualization. *Bioinformatics* **31**:2382-2383.  
1335 10.1093/bioinformatics/btv145.
- 1336 **Yu, G.C., Wang, L.G., Han, Y.Y., and He, Q.Y.** (2012). clusterProfiler: an R Package for  
1337 Comparing Biological Themes Among Gene Clusters. *Omics* **16**:284-287.  
1338 10.1089/omi.2011.0118.
- 1339 **Yuan, Z., Persson, S., and Zhang, D.** (2020). Molecular and genetic pathways for optimizing  
1340 spikelet development and grain yield. *aBIOTECH* **1**:276-292. 10.1007/s42994-020-00026-x.
- 1341 **Zhang, B., Liu, X., Xu, W., Chang, J., Li, A., Mao, X., Zhang, X., and Jing, R.** (2015).  
1342 Novel function of a putative MOC1 ortholog associated with spikelet number per spike in  
1343 common wheat. *Sci Rep* **5**:12211. 10.1038/srep12211.
- 1344 **Zhang, D.B., and Yuan, Z.** (2014). Molecular Control of Grass Inflorescence Development.  
1345 *Annu Rev Plant Biol* **65**:553-578. 10.1146/annurev-arplant-050213-040104.
- 1346 **Zhang, L., Zhang, H., Qiao, L.Y., Miao, L.F., Yan, D., Liu, P., Zhao, G.Y., Jia, J.Z., and**  
1347 **Gao, L.F.** (2021). Wheat MADS-box gene TaSEP3-D1 negatively regulates heading date. *Crop*  
1348 **J** **9**:1115-1123. 10.1016/j.cj.2020.12.007.
- 1349 **Zhang, Y., Liu, T., Meyer, C.A., Eeckhoute, J., Johnson, D.S., Bernstein, B.E., Nusbaum,**  
1350 **C., Myers, R.M., Brown, M., Li, W., et al.** (2008). Model-based analysis of ChIP-Seq  
1351 (MACS). *Genome Biol* **9**:R137. 10.1186/gb-2008-9-9-r137.
- 1352 **Zhao, L., Lin, X., Yang, Y., Bie, X., Zhang, H., Chen, J., Liu, X., Wang, H., Jiang, J., Fu,**  
1353 **X., et al.** (2022). Chromatin reprogramming and transcriptional regulation orchestrate  
1354 embryogenesis in hexaploid wheat. *bioRxiv* <https://doi.org/10.1101/2022.01.21.477188>.
- 1355 **Zhou, Y., Zhao, X.B., Li, Y.W., Xu, J., Bi, A.Y., Kang, L.P., Xu, D.X., Chen, H.F., Wang,**  
1356 **Y., Wang, Y.G., et al.** (2020). Triticum population sequencing provides insights into wheat  
1357 adaptation. *Nature Genetics* **52**:1412-1422. 10.1038/s41588-020-00722-w.
- 1358 **Zhu, W.W., Yang, L., Wu, D., Meng, Q.C., Deng, X., Huang, G.Q., Zhang, J., Chen, X.F.,**  
1359 **Ferrandiz, C., Liang, W.Q., et al.** (2022). Rice SEPALLATA genes OsMADS5 and  
1360 OsMADS34 cooperate to limit inflorescence branching by repressing the TERMINAL  
1361 FLOWER1-like gene RCN4. *New Phytologist* **233**:1682-1700. 10.1111/nph.17855.
- 1362  
1363  
1364

1365 **Supplemental Figures**



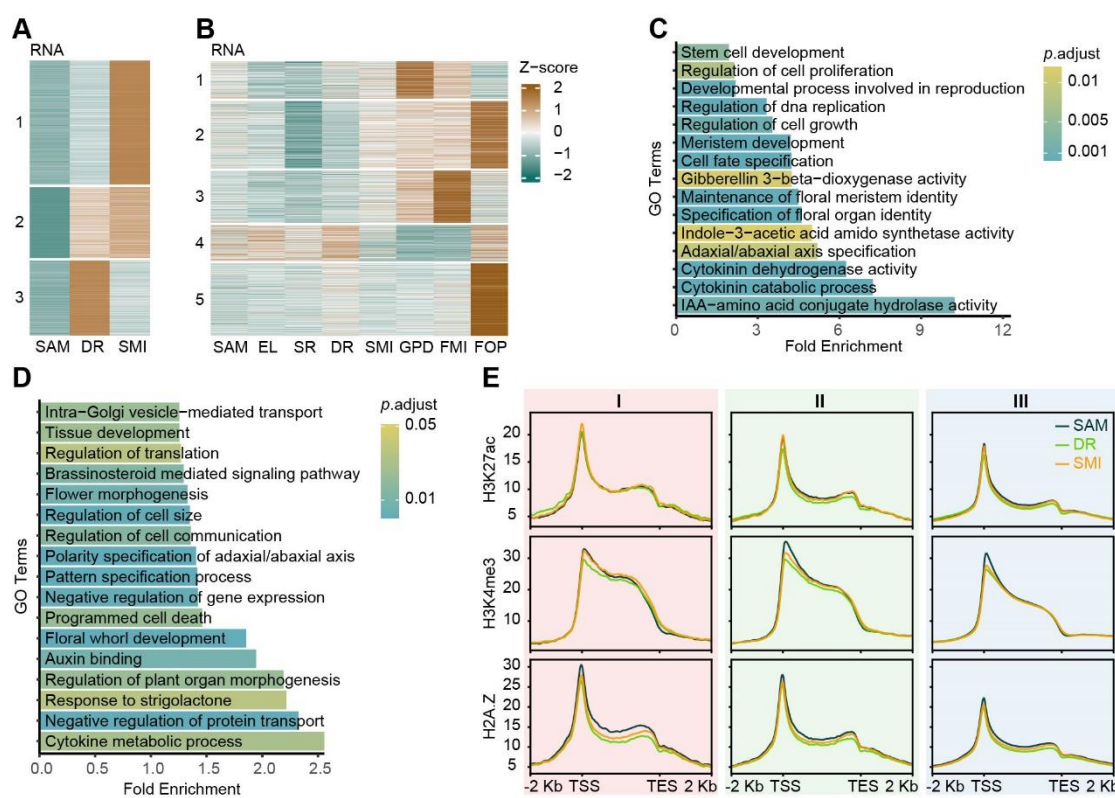
1366

1367 **Supplemental Figure 1. Features of various histone modifications.**

1368 (A) IGV browser view at *TaDEP1* locus showing various epigenomic data types at  
1369 stages and transcriptome levels of different sampling stages.

- 1370 (B) Correlation between different types of histone modification profiles and gene  
1371 expression levels.  
1372 (C) Cluster dendrogram of ATAC-seq data showing five distinct development clusters:  
1373 vegetative cluster (SAM, EL, SR), flowering transition stage (DR), inflorescence  
1374 initiation (SMI), spikelet meristem formation (GPD, FMI) and floret meristem  
1375 formation (FOP).  
1376 (D) The matrix of differentially accessible regions (DARs) numbers among  
1377 developmental stages. The number of decreased and increased chromatin  
1378 accessibility compared with former stages were represented in the lower-triangle  
1379 (number in light blue) and upper-triangle panel (number in light red), respectively.  
1380 A region with  $|\log_2(\text{Fold Change})| \geq 1$  and  $\text{FDR} \leq 0.05$  by DiffBind between any  
1381 two stages was considered as DAR.  
1382 (E) Pair-wise correlation map among different histone modification profiles. Jaccard  
1383 index was calculated based on the peaks overlap, and then Pearson correlation scores  
1384 were generated.  
1385 (F-H) PCA of H2A.Z (F), H3K36me3 (G) and H3K4me3 (H) samples during spike  
1386 development. Each dot represents one sample; two bio-replicates are sequenced for  
1387 each stage.

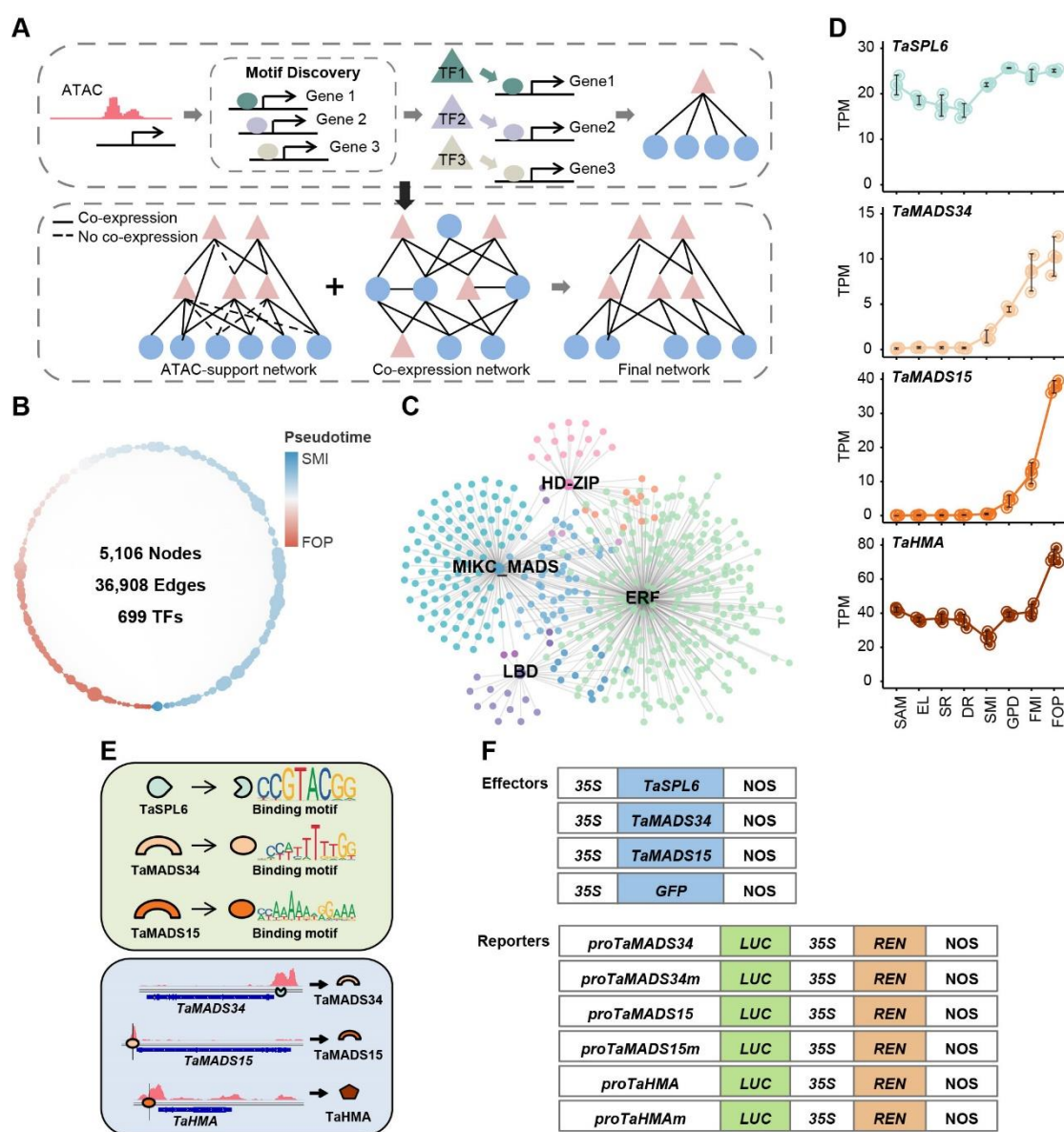
1388



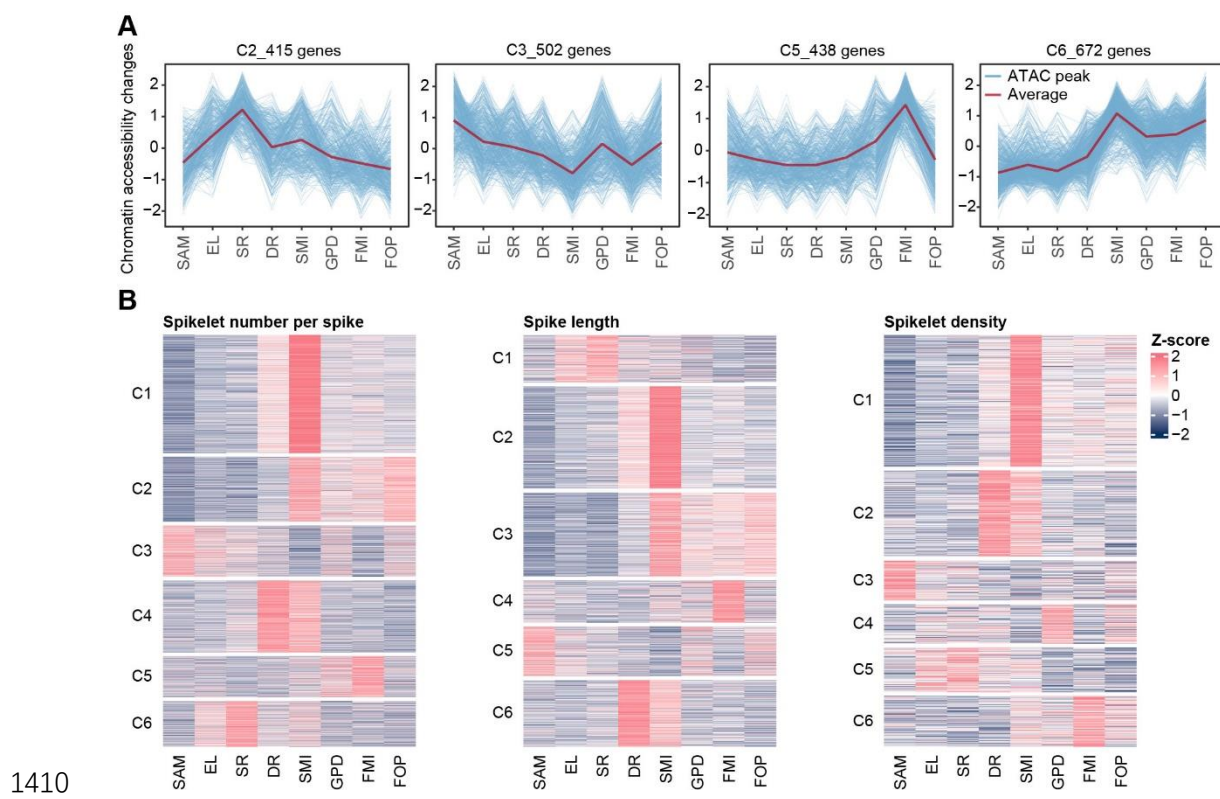
1389

- 1390 **Supplemental Figure 2. Chromatin landscape dynamics associates with**  
1391 **transcriptional change from vegetative to reproductive transition.**  
1392 (A and B) Expression pattern of genes up-regulated at DR and SMI stage versus SAM  
1393 stage (A) and genes up-regulated at later stages rather than DR or SMI stages (B).  
1394 Heatmap showing k-mean clustering of gene expression.

1395 (C and D) GO enrichment analysis of genes in gene set II (C), III (D) in Figure 2C.  
 1396 (E) H3K27ac (top), H3K4me3 (middle) and H2A.Z (bottom) levels of genes in gene  
 1397 set I, II, III in Figure 2C at SAM, DR and SMI stages.  
 1398



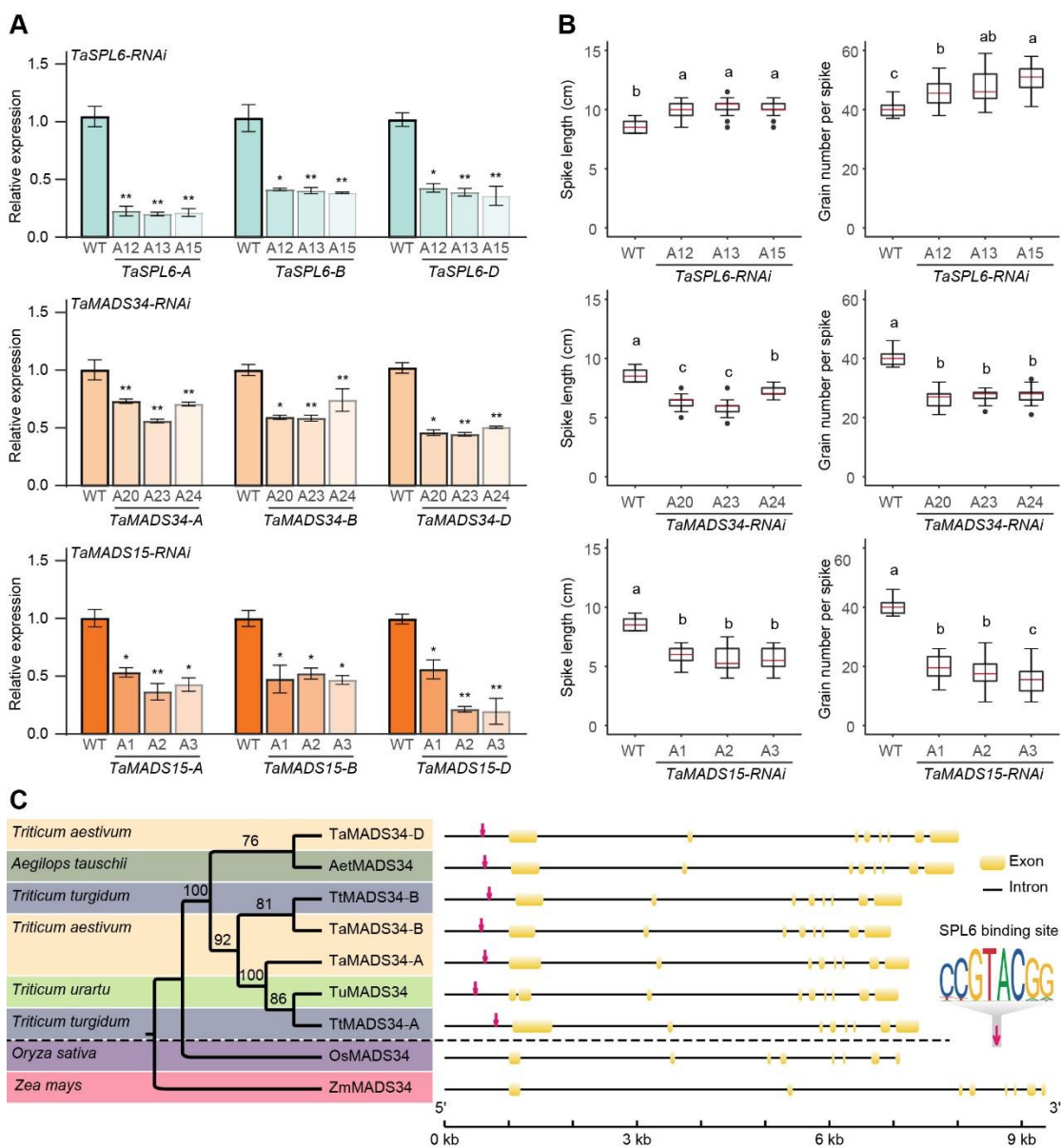
1399  
 1400 **Supplemental Figure 3. Construction of transcription regulatory network (TRN).**  
 1401 (A) Schematic of the strategy for TRNs building (see method for detail).  
 1402 (B) Total TRNs characterized for governing spike architecture formation.  
 1403 (C) Map view of TF-targets for different TF families.  
 1404 (D) Dynamic expression profile of *TaSPL6*, *TaMADS34*, *TaMADS15* and *TaHMA* at  
 1405 different stages during spike development.  
 1406 (E) Presence of different TF binding motifs in the target gene's open chromatin regions  
 1407 from the SPL6-MADS34-MADS15-HMA regulatory module.  
 1408 (F) Schematic diagram showing the vectors used in the Luciferase reporter assays of  
 1409 Figure 3H.



1411 **Supplemental Figure 4. The chromatin accessibility dynamics of GWAS signal  
1412 associated genes.**

1413 (A and B) K-means clustering of chromatin accessibility of fertile spikelet number per  
1414 spike (FSPS) (A), spikelet number per spike (SNS) (left-B), spike length(SL)  
1415 (middle-B), spikelet density (SD) (right-B) related genes during spike  
1416 development.

1417



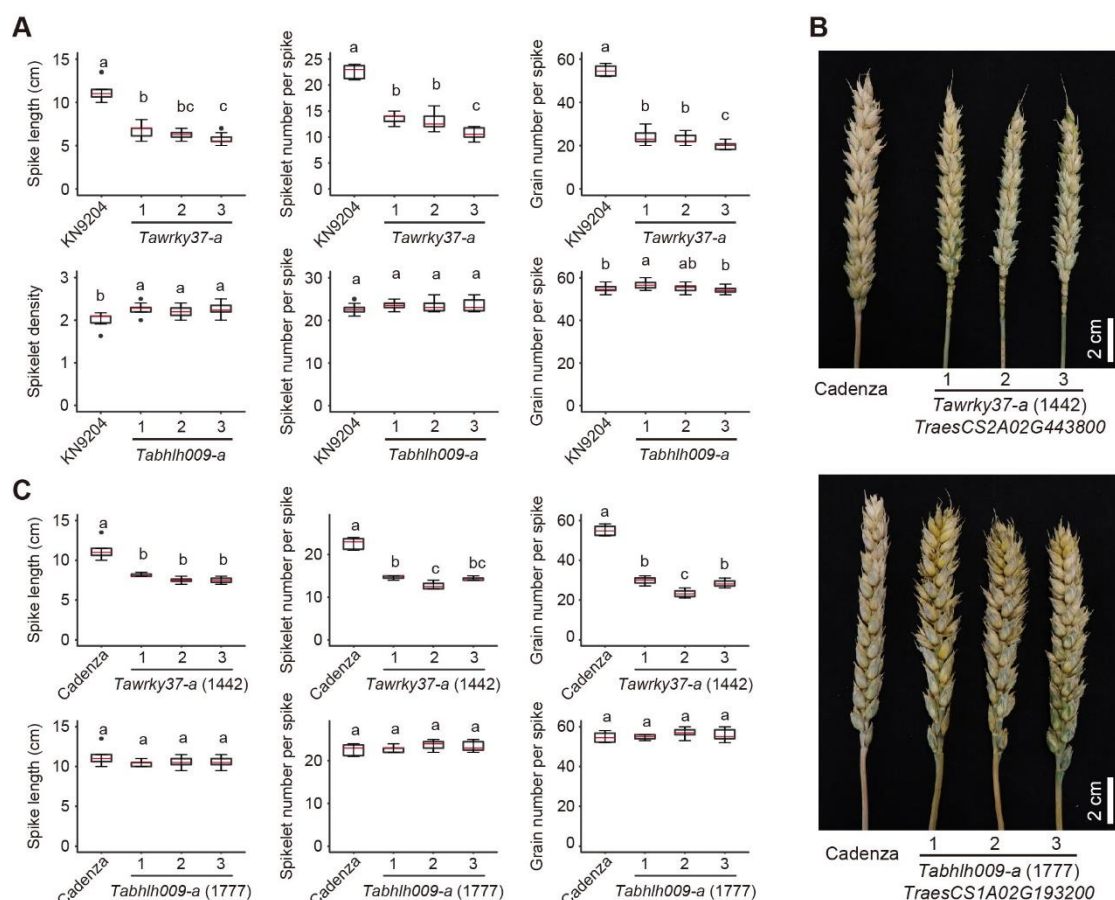
1418

1419 **Supplemental Figure 5. SPL6-MADS34-MADS15-HMA module affects spike**  
 1420 **development in wheat.**

- 1421 (A) The knock-down efficiency of target genes in different *TaSPL6-RNAi*, *TaMADS34-*  
 1422 *RNAi*, *TaMADS15-RNAi* transgenic plants as measured by qPCR. Fielder served  
 1423 as wild-type (WT). Expression level of genes in WT is set as 1.0, the relative  
 1424 expression of each gene in RNAi plants is shown as average  $\pm$  SD of three  
 1425 replicates. Student's *t* test was used for the statistical significance (\*,  $p \leq 0.05$ ; \*\*,  
 1426  $p \leq 0.01$ ).
- 1427 (B) Quantification of spike length, grain number per spike (GNPS) between WT,  
 1428 *TaSPL6-RNAi*, *TaMADS34-RNAi* and *TaMADS15-RNAi* transgenic plants. Two-  
 1429 tailed Student's *t*-tests. In box plots, the box limits indicate the 25th and 75th  
 1430 percentiles, the whiskers indicate the full range of the data, and the centre line  
 1431 indicates the median. Different letters mean significant difference at  $p < 0.01$ .

1432 (C) TaSPL6 binding motif (CCGTACGG) at chromatin accessible region of *MADS34*  
 1433 orthologs in different *Triticum* was conserved, but not in *Oryza sativa* or *Zea*  
 1434 *mays*. Phylogenetic tree of corresponding species is indicated on the left.  
 1435 Schematic diagram of gene structure and presence or absence of SPL6 binding  
 1436 motif sites is shown on the right.

1437



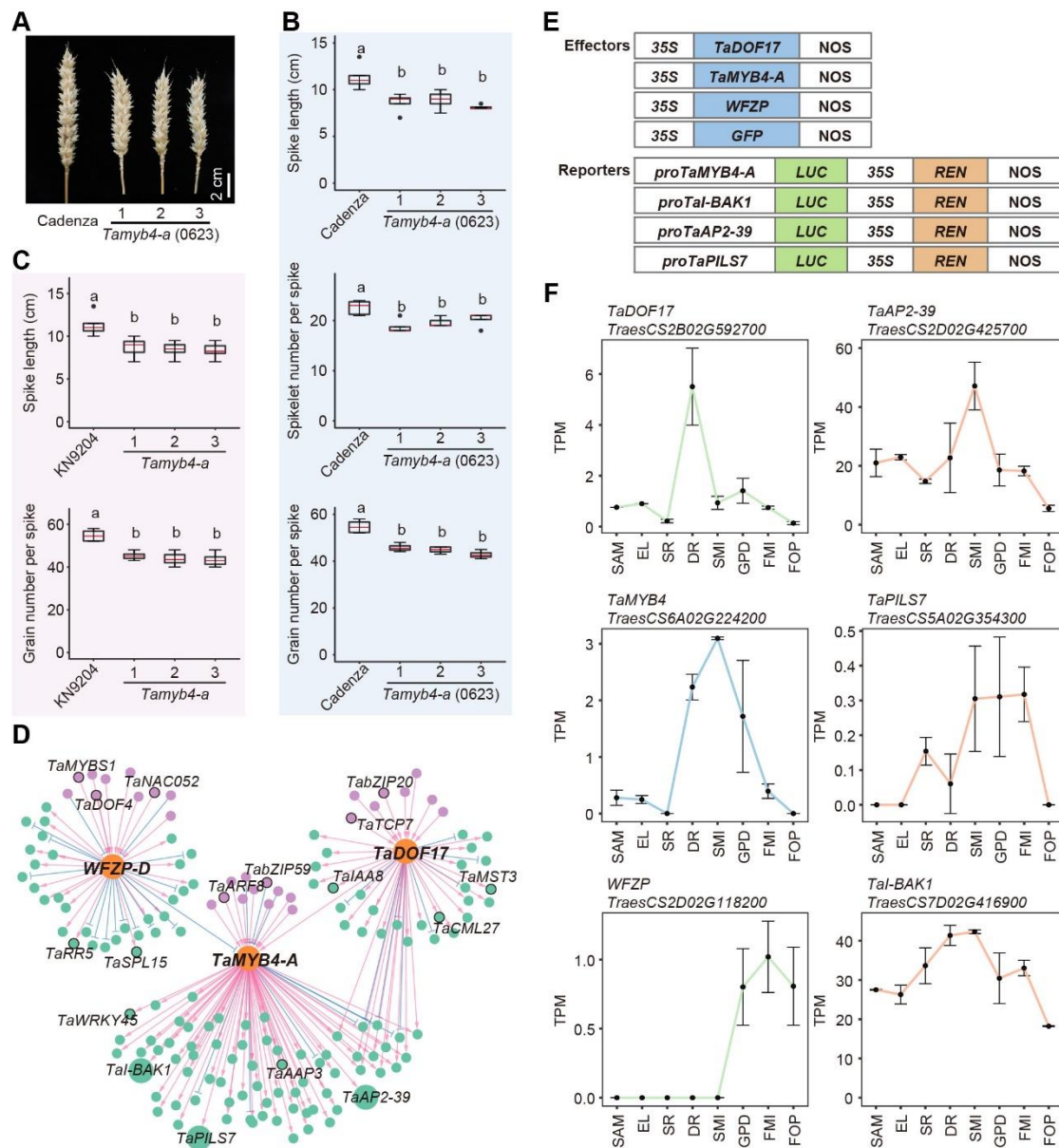
1438

1439 **Supplemental Figure 6. The quantification data of spike phenotype associated  
 1440 with novel factors mutations.**

- 1441 (A) Quantification of spike length, spikelet number per spike (SNS), gain number per  
 1442 spike (GNPS) for represented KN9204 TILLING lines containing mutation of  
 1443 *Tabhlh009-a* or *Tawrky37-a*. Two-tailed Student's *t*-tests. In box plots, the box  
 1444 limits indicate the 25th and 75th percentiles, the whiskers indicate the full range  
 1445 of the data, and the centre line indicates the median. Different letters mean  
 1446 significant difference at  $p < 0.01$ .
- 1447 (B) The spike developmental defect of *TraesCS2A02G443800* (*TaWRKY37-A*, line  
 1448 1442) and *TraesCS1A02G193200* (*TabHLH009-A*, line 1777) mutant lines as  
 1449 compared to control Cadenza. Scale bars =2 cm.
- 1450 (C) Quantification of spike length, spikelet number per spike (SNS), gain number per  
 1451 spike (GNPS) for represented Cadenza TILLING lines containing mutation of  
 1452 1442 (*TaWRKY37-A*, *TraesCS2A02G443800*) and 1777 (*TabHLH009-A*,  
 1453 *TraesCS1A02G193200*). Two- tailed Student's *t*-tests. In box plots, the box limits

1454 indicate the 25th and 75th percentiles, the whiskers indicate the full range of the  
 1455 data, and the centre line indicates the median. Different letters mean significant  
 1456 difference at  $p < 0.01$ .

1457



1458

1459 **Supplemental Figure 7. The regulation network of TaMYB4-A of wheat spike  
 1460 architecture.**

- 1461 (A) Comparison of the spike phenotype of Wild-type (Cadenza) and mutant lines from  
 1462 Cadenza mutant library 0623 (*TaWRKY37-A*, *TraesCS2A02G443800*). Scale bars  
 1463 = 2 cm.
- 1464 (B) Statistics comparison of spike length and spikelet number per spike (SNS) between  
 1465 Wild-type (Cadenza) and 0623 (*TaWRKY37-A*, *TraesCS2A02G443800*) mutant  
 1466 lines. Two-tailed Student's *t*-tests. In box plots, the box limits indicate the 25th  
 1467 and 75th percentiles, the whiskers indicate the full range of the data, and the centre  
 1468 line indicates the median. Different letters mean significant difference at  $p < 0.01$ .

- 1469 (C) Statistics comparison of spike length and grain number per spike (GNPS) between  
1470 KN9204 and *Tamyb4-a* mutant lines. Two-tailed Student's *t*-tests. In box plots, the  
1471 box limits indicate the 25th and 75th percentiles, the whiskers indicate the full  
1472 range of the data, and the centre line indicates the median. Different letters mean  
1473 significant difference at  $p < 0.01$ .
- 1474 (D) The transcription regulatory network (TRN) of *TaMYB4-A*.
- 1475 (E) Schematic diagram showing the vectors used in the Luciferase reporter assays of  
1476 *TaMYB4-A* regulatory network of Figure 7F.
- 1477 (F) The expression level of *TaDOF17*, *TaMYB4-A*, *WFZP*, *TaAP2-39*, *TaI-BAK1*,  
1478 *TaPILS7*.